The 11 year solar cycle signal in transient simulations from the Whole Atmosphere Community Climate Model

G. Chiodo,[1] N. Calvo,[2] D. R. Marsh,[2] and R. Garcia-Herrera[3]

Received 13 June 2011; revised 3 February 2012; accepted 9 February 2012; published 29 March 2012.

[1] The atmospheric response to the 11 year solar cycle (SC) and its combination with the quasi-biennal oscillation (QBO) are analyzed in four simulations of the Whole Atmosphere Community Climate Model version 3.5 (WACCM3.5), which were performed with observed sea surface temperatures, volcanic eruptions, greenhouse gases, and a nudged QBO. The analysis focuses on the annual mean response of the model to the SC and on the evolution of the solar signal during the Northern Hemispheric winter. WACCM3.5 simulates a significantly warmer stratosphere under solar maximum conditions compared to solar minimum. The vertical structure of the signal in temperature and ozone at low latitudes agrees with observations better than previous versions of the model. The temperature and wind response in the extratropics is more uncertain because of its seasonal dependence and the large dynamical variability of the polar vortex. However, all four simulations reproduce the observed downward propagation of zonal wind anomalies from the upper stratosphere to the lower stratosphere during boreal winter resulting from solar-induced modulation of the polar night jet and the Brewer-Dobson circulation. Combined QBO-SC effects in the extratropics are consistent with observations, but they are not robust across the ensemble members. During boreal winter, solar signals are also found in tropospheric circulation and surface temperature. Overall, these results confirm the plausibility of proposed dynamical mechanisms driving the atmospheric response to the SC. The improvement of the model climatology and variability in the polar stratosphere is the basis for the success in simulating the evolution and magnitude of the solar signal.

Citation: Chiodo, G., N. Calvo, D. R. Marsh, and R. Garcia-Herrera (2012), The 11 year solar cycle signal in transient simulations from the Whole Atmosphere Community Climate Model, *J. Geophys. Res.*, *117*, D06109, doi:10.1029/2011JD016393.

1. Introduction

[2] The influence of the solar cycle (SC) on climate is a research topic of high scientific relevance because of the need of estimating and separating natural variability from anthropogenic climate change. This challenge is hampered by the lack of understanding in the physical mechanisms involved in the atmospheric response to variations in solar flux, such as those over the 27 day rotational period, and the 11 year SC.

[3] The measured total change in solar irradiance during the 11 year SC is around 0.1%, translating into a radiative forcing of 0.2–0.3 W m^{-2} in the total solar irradiance (TSI). Although the net forcing in the TSI is small, measurements from space indicate large variations (4%–8%) in the UV range of 200–250 nm from solar minima to maxima conditions [*Lean et al.*, 1997]. The increase in UV irradiance modulates stratospheric ozone and oxygen photolysis, in a way that ozone concentration increases in the upper and middle stratosphere during solar maximum. Strong absorption of UV radiation by the additional ozone augments the temperature response in the upper stratosphere, thus providing an amplification mechanism for the response in temperature [*McCormack and Hood*, 1996; *Shindell et al.*, 1999].

[4] Satellite observations and reanalysis data show that the strongest variations in ozone associated with the 11 year SC occur in the upper tropical stratosphere [*Hood et al.*, 1993; *McCormack and Hood*, 1996; *Soukharev and Hood*, 2006; *Randel and Wu*, 2007]. In addition, a significant increase is also found in the lower tropical stratosphere. This leads to a double-peak structure in the vertical profile of the ozone response at low latitudes [*Soukharev and Hood*, 2006]. The impact of the 11 year SC has also been observed in zonal mean temperature and winds. Satellite and reanalysis data sets show a significant warming in the upper tropical stratosphere [*Frame and Gray*, 2010; *Gray et al.*, 2010]. However, the signals in temperature are not confined to the upper stratosphere. A warming response was also observed in the lower tropical stratosphere [*Labitzke and Van Loon*, 1995]. These responses were also evident when data

[1]Departamento Fisica de la Tierra II, Facultad de Ciencias Fisicas, Universidad Complutense de Madrid, Madrid, Spain.
[2]Atmospheric Chemistry Division, National Center for Atmospheric Research, Boulder, Colorado, USA.
[3]Agencia Estatal de Meteorologia, Madrid, Spain.

0148-0227/12/2011JD016393

covering an additional solar cycle became available [*Crooks and Gray*, 2005], and when the effect of volcanic eruptions was adequately separated [*Frame and Gray*, 2010]. Solar signals in temperature and zonal wind were also documented during boreal winter in the extratropical lower stratosphere [*Crooks and Gray*, 2005; *Frame and Gray*, 2010]. In addition, NCEP reanalysis and model simulations suggest that peaks of solar activity lead to a poleward shift of the subtropical tropospheric jet and to a broadening of the Hadley circulation [*Haigh and Blackburn*, 2006].

[5] The solar-induced temperature changes in the upper tropical stratosphere are caused by a direct response to the increase in UV radiation. The response in the other atmospheric regions (e.g., in the lower equatorial and extratropical stratosphere) is an indirect result of dynamical changes in stratospheric and tropospheric circulation. During boreal winter, a poleward and downward propagation of solar signals in zonal wind has been observed in the extratropical stratosphere [*Kuroda and Kodera*, 2002]. Accordingly, it seems plausible that the radiatively driven signal in the upper tropical stratosphere propagates to the lower stratosphere and to the troposphere via dynamical processes, so that the 11 year SC can influence the lower atmosphere via a "top-down" pathway [*Matthes et al.*, 2006; *Meehl et al.*, 2009]. In addition, *Meehl et al.* [2009] suggest that the impact of the SC in the troposphere could also be originated by a "bottom-up" pathway involving ocean-atmosphere feedbacks in the Pacific region.

[6] Although a unique and definitive mechanism has not been identified yet for both pathways, for the top-down response, there is general consensus on two hypothesized processes controlling the downward propagation of the SC signals in temperature and zonal wind [*Kodera and Kuroda*, 2002]: (1) the modulation of the polar night jet (PNJ) oscillation and (2) changes of the Brewer-Dobson circulation. These processes are driven by a combination of direct (radiative) and indirect (dynamical) effects in the stratosphere, which operate during winter months in both hemispheres.

[7] However, interactions between the SC and other modes of stratospheric variability, e.g., the quasi-biennial oscillation (QBO) and El Niño–Southern Oscillation (ENSO), complicate the overall picture. Several observational studies indicated that correlations of solar activity with winter temperatures in the lower extratropical stratosphere increase substantially in February when the data is stratified according to the QBO phase [*Labitzke*, 1987; *Labitzke and Van Loon*, 1989; *Labitzke*, 2004]. A similar QBO-SC relationship was also found in the low equatorial stratosphere [*Labitzke*, 2005]. These combined QBO-SC effects seem to depend on the state of the winds in the upper stratosphere, as suggested by *Gray et al.* [2004], where QBO and solar influences may enhance or counteract each other. Nevertheless, the detailed physical mechanism which originates this relationship remains unclear.

[8] Additionally, the characterization of the observed solar signal is hampered by limitations in the length and quality of the observational data sets and the statistical analysis. Reanalysis from NCEP-NCAR [*Kalnay et al.*, 1996; *Kistler et al.*, 2001] and ERA-40 [*Uppala et al.*, 2005] cover the last five solar cycles (1950–2009). However, reliable satellite data covering altitudes above 10 hPa became available for assimilation in 1978. Hence, the assimilation systems have only been constrained with stratospheric observations for a time span covering the last three cycles (1978–2009).

[9] Such a limited reference period might complicate the attribution of decadal variability to the SC because of the contamination of the solar signal with that from other sources of variability as, e.g., volcanic aerosols [*Lee and Smith*, 2003], ENSO [*Marsh and Garcia*, 2007], and QBO [*Smith and Matthes*, 2008]. In addition, previous observational studies were generally based on linear statistical methods like regression models, which are methods that cannot, by definition, account for the nonlinear interactions mentioned above.

[10] A whole range of atmospheric models has been used in the past to simulate the stratospheric and tropospheric response to solar variability. Pioneering work was done with 2-D models with interactive photochemistry [*Huang and Brasseur*, 1993; *Haigh*, 1994; *Fleming et al.*, 1995]. Improved versions of 2-D models with interactive photochemistry and dynamics were used to determine possible aliasing effects in the observed 11 year SC signals in ozone and temperature in the lower stratosphere due to the QBO and volcanic events [*Lee and Smith*, 2003; *Smith and Matthes*, 2008]. However, these models lacked a full description of wave-mean flow interactions that have been proposed to be the origin of these signals.

[11] Further improvements were made by using GCMs with interactive chemistry (hereafter chemistry-climate models (CCMs)) [*Tourpali et al.*, 2003; *Rozanov et al.*, 2004; *Egorova et al.*, 2004; *Marsh et al.*, 2007; *Schmidt et al.*, 2010; *Matthes et al.*, 2010]). Despite advances in model physics, the improvement of CCMs over 2-D models in reproducing the observed solar signal in temperature and ozone was only partial [*Labitzke et al.*, 2002], particularly in the tropical lower stratosphere. The reasons for this are still unclear, although CCMs still presented limitations, as the absence of an internally generated QBO (e.g., the models used by *Tourpali et al.* [2003], *Egorova et al.* [2004], and *Marsh et al.* [2007]), the use of perpetual maximum and minimum solar activity conditions [e.g., *Marsh et al.*, 2007; *Schmidt et al.*, 2010], or climatological SSTs as boundary conditions [e.g., *Tourpali et al.*, 2003; *Egorova et al.*, 2004; *Matthes et al.*, 2004]. Some of the CCMs simulate a significant response in the polar vortex during boreal winter in the NH [*Matthes et al.*, 2004; *Rozanov et al.*, 2004; *Schmidt et al.*, 2010]. However, the observed magnitude and seasonal march of the extratropical signals in zonal wind and temperature were not reproduced by these models.

[12] Another limitation of most previous modeling studies, when the analysis was extended to the extratropics and focused on the seasonal evolution of the solar signal in zonal wind and temperature, was the use of single simulations instead of an ensemble [e.g., *Matthes et al.*, 2004; *Tsutsui et al.*, 2009; *Schmidt et al.*, 2010]. The significance of the simulated solar signals is then generally small because of the high levels of variability, especially at high latitudes. In an experimental design with transient forcings, the use of ensembles leads to a better estimate of the model variability, and thus of the significance of the solar signal.

[13] In this paper we present the analysis of the 11 year solar signal in four-member ensemble of simulations from a "whole atmosphere" CCM incorporating an assimilated QBO: version 3.5 of the Whole Atmosphere Community

Climate Model (WACCM3.5). The simulations were performed with all observed forcings for the reference period 1960–2005, including prescribed SSTs as boundary conditions, which allows for direct comparison with observations. The model has a well resolved stratosphere and a vertical domain extending to 145 km, which leads to better representation of wave-mean flow interactions, and makes the model particularly suited for investigating the top-down solar-induced response. Accordingly, analysis of both the composited ensemble mean and each ensemble member reveals a robust solar signal in the upper stratosphere that propagates to the troposphere via wave-mean flow interactions during Northern Hemisphere (NH) winter, consistent with previously proposed mechanisms. Our results show that the simulated response in the tropical lower stratosphere is linked to the evolution of the extratropical SC signal.

[14] The paper is arranged as follows. Section 2 provides a description of the model, the experimental design and the statistical methods employed to extract the SC signal in different fields (e.g., ozone). The simulated annual mean response to the SC is presented in section 3. In section 4, the analysis is refined to monthly timescales, and dynamical mechanisms are explored. Section 5 summarizes the main results and conclusions.

2. Data and Methodology

2.1. Model and Experimental Design

[15] WACCM3.5 is an improved version of the WACCM3.1 global circulation model [*Garcia et al.*, 2007]. It has 66 vertical levels which extend from the surface to the thermosphere (145 km). Since the vertical model layers are based on a hybrid pressure–sigma coordinate system, the vertical resolution is variable, and ranges from approximately 1 km in the mid troposphere to about 3.5 km in the upper mesosphere. The underlying GCM is based on CAM3 [*Collins et al.*, 2004] and uses a finite-volume dynamical core [*Lin*, 2004] with 1.9° longitude by 2.5° latitude horizontal resolution. In the simulations analyzed here, WACCM3.5 was run coupled with a fully interactive chemistry module (details are given by *Kinnison et al.* [2007]) that includes neutral and ionized species. In addition to photoionization by extreme ultraviolet radiation, the model includes ionization by energetic particle precipitation events in the auroral regions, as explained by *Marsh et al.* [2007]. This leads to a more accurate representation of thermospheric nitric oxide, which might also be transported to the upper stratosphere, affecting ozone concentrations and heating rates [*Marsh et al.*, 2007].

[16] The major code changes from WACCM3.1 to WACCM3.5 relate to the gravity wave (GW) physics. The triggering of GW near the tropopause is driven by a more physically based parameterization [*Richter et al.*, 2009] than in WACCM3.1. *Richter et al.* [2009] showed that the change in GW physics leads to a more realistic winter stratospheric jet in WACCM3.5 compared to the previous version WACCM3.1. Furthermore, they showed that the inclusion of a turbulent mountain stress term to estimate surface stress due to unresolved orography has a large impact on the simulated frequency of major sudden stratospheric warmings (SSWs). The frequency of major SSWs in WACCM3.5 simulations is reported to be 0.6 events per year (yr^{-1}), which is in agreement with ERA-40 (0.6 yr^{-1}), while WACCM3.1 shows a much lower frequency (0.1 yr^{-1}) [*Richter et al.*, 2009].

[17] For the solar spectral irradiance at wavelengths greater than 121 nm (Lyman-α), photolysis and photoionization rates are calculated directly using the spectral irradiance modeled by *Lean et al.* [2005], according to the recommendations for the second CCM Validation Activity (CCMVal-2) from the Stratospheric Processes and their Role in Climate (SPARC) project. The radiative flux is obtained by integrating the spectral irradiance data over specific bands, and is used as input for both the chemistry and radiation modules. This replaces the implementation of the spectral irradiance in the WACCM3.1 model, in which the solar radiation shortward of 350 nm was inferred from the $F_{10.7}$ index (the details are given by *Marsh et al.* [2007]). For the extreme ultraviolet spectral range (wavelengths between 0.05 nm and 121 nm), the Solomon and Qian parameterization [*Solomon and Qian*, 2005] is used to calculate the solar irradiance and the solar variability factor, as in WACCM3.1. More details of the parameterization, along with the photochemistry of the model, are given by *Marsh et al.* [2007].

[18] We use an ensemble of four simulations of the WACCM3.5 model run from 1960 to 2005, whose design differs only in the initial conditions. The simulations were run with observed forcings, which comprise spectrally resolved solar variability, observed SSTs and sea ice concentrations, loadings of GHG and ozone depleting substances. Model equatorial stratospheric winds were relaxed toward observed winds to obtain a realistic time-varying QBO oscillation [*Matthes et al.*, 2010]. The effects of volcanic eruptions are simulated by prescribing the surface area density of sulphate aerosols. The assumed aerosol mass distribution is then used along with all other radiatively active gases for the calculation of heating and cooling rates (more details are given by *Tilmes et al.* [2009]).

[19] The imposed SSTs and zonal winds in the tropical stratosphere that follow observations may contain decadal perturbations, which are not related to solar variability. Thus, the responses attributed to the SC may contain signals arising from other sources of variability (i.e., aliasing from decadal changes in ENSO and QBO). On the other hand, nonlinear interactions between changes due to solar variability and other sources of variability would only be captured in such an approach. The inclusion of observed SSTs and QBO variations leads to a more realistic representation of the variability in the simulated climate, particularly in the extratropical stratosphere [*Sassi et al.*, 2004]. This also possibly leads to a higher level of realism in the simulation of solar signals, as part of natural variability in the climate system.

[20] The simulations are part of the CCMVal-2. The results of this activity revealed that the WACCM3.5 climatological global mean temperature and its long-term trends in the stratosphere are in good agreement with observations, and the model accurately represents the annual mean and the annual cycle in ozone and global column ozone [*Austin et al.*, 2010]. WACCM3.5 is also successful in reproducing the stratospheric mean state of the NH, while in the Southern Hemisphere (SH) problems were reported concerning the strength of the stratospheric jet and the cold bias in SH

spring. This bias in the SH is linked to a late vortex breakdown, which indicates that the winter state in this hemisphere lasts too long [*Butchart et al.*, 2010; *Eyring et al.*, 2010]. In the NH, both the shape and the interannual variability of the stratospheric jet are improved in WACCM3.5 compared to previous versions of the model, and the bias in strength was reduced from 20 to 10 m/s [*Richter et al.*, 2009]. The report also showed that WACCM3.5 reproduces a realistic solar signal in temperature and ozone. However, their work on the solar signal was only based on one of the four ensemble realizations (K. Matthes, personal communication 2010), and the annual mean model response was only analyzed in the tropics [*Manzini et al.*, 2010].

2.2. Statistical Methods

[21] The inclusion of all types of observed forcings in a model simulation, as outlined above for WACCM3.5, allows direct comparison with observations but complicates the task of attributing certain signals to solar variability. For this reason, we examined the solar-induced response with two different statistical methods which are in common use in the literature: multiple linear regression (MLR) and composite analysis. Nonlinear interactions with other sources of variability have been reported to occur in the extratropics [*Calvo et al.*, 2009; *Calvo and Marsh*, 2011]. Therefore, composites are preferred over the regression for the analysis of the signal in the extratropical stratosphere during winter.

2.2.1. Multiple Linear Regression

[22] The solar signal is often calculated in observations and model simulations by means of linear regression methods, in which the predictors represent the forcings included in the simulations. For comparison purposes with previous studies, we also adopt the standard MLR technique, and regress monthly and annual mean fields onto different predictors, which are consistent with the design of the WACCM3.5 simulations:

$$\mathrm{Var} = b_0 + b_1 t + b_2 \mathrm{AOD} + b_3 F_{10.7a} + b_4 \mathrm{QBO}_1(\mathrm{EOF1}) + b_5 \mathrm{QBO}_2(\mathrm{EOF2}) + b_6 N3.4(t - \mathrm{lag}_{\mathrm{ENSO}}) \quad (1)$$

[23] We include a constant factor (b_0), a long-trend term, the 11 year SC, the QBO, an ENSO-term and a volcanic aerosol term in the statistical fit. A least squares linear trend is used to compute the long-term trend, while a 80 days centered mean of the daily values of the solar radio flux ($F_{10.7a}$) is used as input for the 11 year SC. The QBO term is calculated with two indexes, which are based on the first and second EOF in the QBO vertical domain [see *Randel and Wu*, 1996], orthogonal by construction. In the regression equation, the aerosol optical depth index (AOD index) is used as a predictor for volcanic effects. We used the data from *Sato et al.* [1993]; since no major eruptions occurred from 2000 until the end of our simulations (2005), no update of the AOD index has been necessary. N3.4 is the NIÑO 3.4 index, which is used as predictor for the ENSO effects. A 3 month lag is chosen to allow for the ENSO signal to propagate to the lower tropical stratosphere [*Garcia-Herrera et al.*, 2006].

[24] The autocorrelation of the residuals is taken into account in our regression analysis by including an autoregressive noise model of first order in the regression equation. The original data set (left-hand side of equation (1)) and the basis function (i.e., the matrix including all regressors) are corrected with the autocorrelation coefficient of the residuals, which is estimated from a first application of the MLR model (more details are given by *Garny et al.* [2007]). The use of this correction leads to more accurate estimates of the regression coefficients and of the 2σ uncertainty level of the fits [*Tiao et al.*, 1990]. We use the 2σ uncertainty from the corrected regression coefficients as a parametric test to assess significance of the solar regression fits.

[25] Even though a separation of the response to the whole set of forcings can be obtained, only the SC signature will be analyzed here. The regression method is only able to capture the linear solar signal. Therefore, nonlinear interactions between QBO and SC, which may be important contributors to the indirect dynamical effects observed in the lower stratosphere at high latitudes [*Labitzke and Van Loon*, 1989], cannot be accounted for.

[26] For better comparison with past observational [*Frame and Gray*, 2010] and modeling [*Austin et al.*, 2008] studies, we use the $F_{10.7}$ flux even though it has not been used to drive the solar variability in the WACCM3.5 model. The solar regression coefficient has also been normalized throughout the figures to a forcing of 100 units of the $F_{10.7}$ radio flux (100 sfu).

2.2.2. Composite Analysis

[27] All months and years in solar maximum and minimum conditions have been grouped together in the same monthly or annual composite whenever the monthly and annual mean observed F10.7 cm radio flux (downloaded from NOAA data service http://www.ngdc.noaa.gov/stp/solar/solardataservices.html) was higher than 145 (for solar maximum) or lower than 95 (for solar minimum).

[28] To examine the combined QBO-SC effects, the model data were also stratified according to the QBO phase. To do so, the equatorial zonal mean zonal wind at 30 hPa was used to define a QBO index. The same criteria used by *Calvo et al.* [2007] to analyze the QBO signature in ERA-40 data were used here. Monthly and annual mean model output were merged into the QBO/WEST or QBO/EAST phase whenever the average of the modeled equatorial zonal mean zonal wind at 30 hPa is higher than 5 m/s, or lower than −10 m/s. Positive values indicate westerly winds, while negative values indicate easterly winds. When studying the SC-QBO signal in the extratropics, an important requisite is that the model reproduces the observed extratropical QBO signal, known as the Holton-Tan (HT) relationship [*Holton and Tan*, 1980]. With the chosen threshold values of zonal wind for QBO/WEST and QBO/EAST conditions, a significant QBO signal computed as difference between QBO/WEST and QBO/EAST months is found during boreal winter in the NH polar vortex (not shown). As shown in Figure 1, the asymmetry of the threshold values for the QBO index follows that in the zonal wind values at the 30 hPa level, where easterly phases are stronger than westerly phases. The monthly mean composites for each solar and QBO phase have been computed as the average of all months included in each group, and differences between composites have been taken to analyze the respective signals. MAX-MIN differences are computed to investigate the pure SC signal, where MAX and MIN stand for solar maximum and

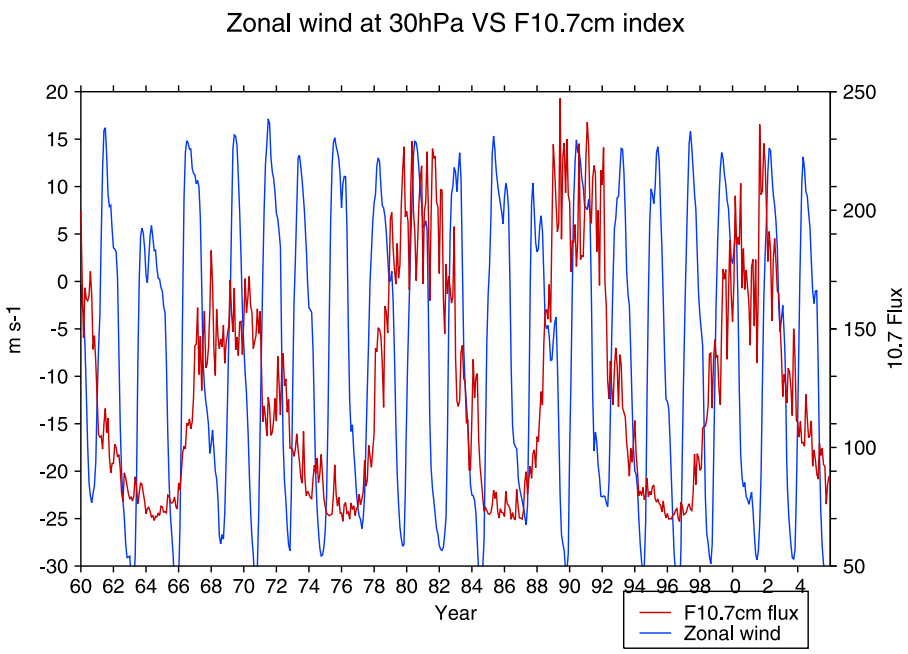

Figure 1. Time series of the zonal mean zonal wind (m/s) at 30 hPa and $F_{10.7}$ flux index during the simulated period (1960–2005).

minimum, respectively. Similarly, MAX-MIN differences have been stratified according to QBO/WEST and QBO/EAST conditions for the study of the SC-QBO signal.

[29] Tables 1 and 2 show the selected years for each SC and for all combinations of QBO and SC phase, respectively. To study the combined SC-QBO effects during NH winter, December has been used as a reference for the QBO phase, so that all winter months were grouped together according to the solar phase and the December zonal wind at 30 hPa. This was done to track the temporal evolution of the solar signal and its modulation by the QBO throughout the NH winter. Before compositing, data were linearly detrended between 1960 and 2005. Furthermore, years with major volcanic eruptions (1982 and 1991) were excluded to avoid aliasing of volcanic signals in the solar response [*Lee and Smith*, 2003]. Since a significant temperature signal caused by the Pinatubo eruption is still detectable approximately 16 months after the eruption event in 1991, the 1992 year was also excluded from the analysis. However, no significant anomalies related to other volcanic eruptions (e.g., Agung in 1963) were detectable in tropical lower stratospheric temperature, thus no more years were excluded from the calculation of composites. Statistical significance of the composite differences has been computed using a Student's *t* test. Throughout this paper, significant values correspond to the 95% confidence level.

Table 1. Years Selected to Compute the Composites for the Maximum (MAX) and Minimum (MIN) Solar Phases in WACCM3.5[a]

	Years
MAX	1960, 1968, 1969, 1970, 1979, 1980, 1981, 1989, 1990, 1999, 2000, 2001, 2002
MIN	1962, 1963, 1964, 1965, 1973, 1974, 1975, 1976, 1977, 1985, 1986, 1987, 1994, 1995, 1996, 1997, 2005

[a]The years 1982, 1991, and 1992 have been excluded from the MAX composite.

3. The Annual Mean Solar Signal

[30] The simulated ensemble mean annual zonal mean temperature and zonal wind responses to the SC have been calculated by means of the regression model described by equation (1). Results for the full reference period, 1960–2005, are shown for both variables in Figures 2a and 2b, respectively. In temperature, a statistically significant warming is evident throughout the stratosphere, characterized by a maximum in the upper stratosphere–lower mesosphere region of up to 0.6 ± 0.2 K/100 sfu at low latitudes, with peak values of 1.4 ± 1.0 K at high latitudes. As it will be shown later, the significant increase in annual mean stratospheric ozone (shown as vertical profile in Figure 4) and the shortwave heating anomalies of 0.2 K/d (not shown) over the upper stratospheric region indicate that the positive temperature signal in the upper stratosphere–lower mesosphere is radiatively driven. In the tropical stratosphere, the

Table 2. Years Selected to Compute the Composites for All Four Combinations of Solar (MAX and MIN) and Quasi-biennial Oscillation (QBO) (QBO/WEST and QBO/EAST) Phases in WACCM3.5

	Years
MAX+QBOW	1969, 1978, 1980, 1988, 1990, 1999, 2002
MIN+QBOW	1964, 1973, 1975, 1985, 1995, 1997
MAX+QBOE	1968, 1970, 1979, 1981, 1989, 2001
MIN+QBOE	1962, 1963, 1965, 1974, 1977,1994, 1996, 2005

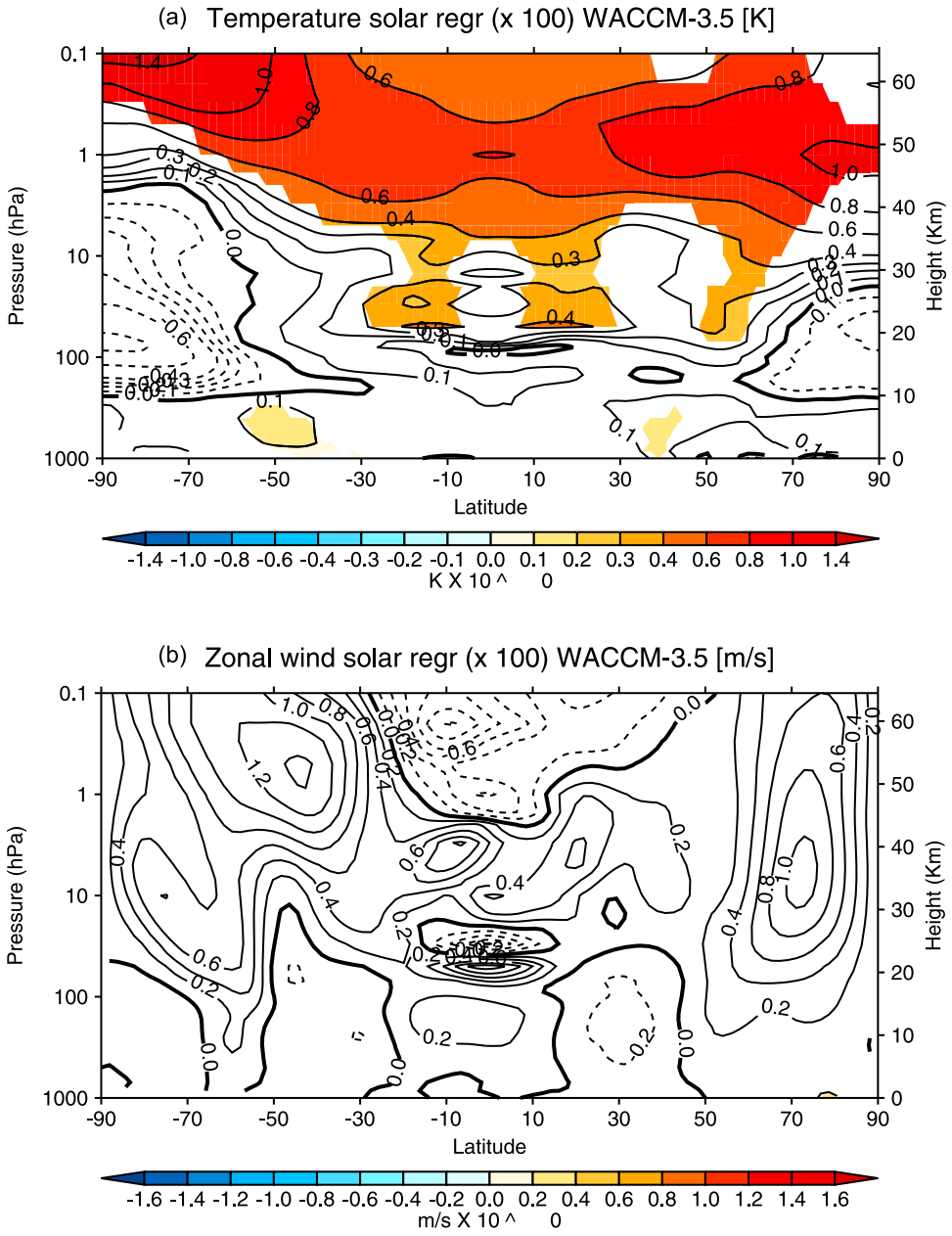

Figure 2. Solar cycle response in (a) zonal mean temperature and (b) zonal mean zonal wind, represented as solar regression coefficient (× 100 sfu) for the full reference period 1960–2005 in WACCM3.5. Colored fields are greater than 2σ. Contours are drawn every 0.1 K. Solid contour lines are drawn to indicate positive values (i.e., warming in Figure 2a and westerly anomalies in Figure 2b), while dashed contours indicate negative values (cooling in Figure 2a and easterly anomalies in Figure 2b).

magnitude of the response gradually decreases with decreasing height, although a statistically significant secondary maximum is found at 20 km. At this altitude, the structure of the response is composed by two separate maxima at subtropical latitudes, with values reaching 0.4 ± 0.1 K/100 sfu. Weaker, but significant, warming areas are also found in the midlatitude troposphere in both hemispheres. In the polar regions the model simulates a weak cooling, though not significant.

[31] It is apparent in Figure 2b that in the annual mean, peaks of solar activity lead to stronger westerlies in both hemispheres. This type of response is expected from the simulated warming at low latitudes on the basis of thermal wind balance. However, the simulated changes are not significant, which is due to the large dynamical variability in the extratropical stratosphere. Weak easterly anomalies are also found in the subtropical troposphere of both hemispheres. As it will be shown in section 4, the tropospheric changes, and the response in the extratropical stratosphere are both seasonally dependent and so lead to a signal in temperature and zonal wind that is only marginally significant in the ensemble mean annual mean.

[32] The results shown above have been calculated on the full available period to obtain a better signal to noise ratio. Nevertheless, the period for which reliable observational data sets exist is more limited than the one analyzed in the model. Even though more than 50 years of reanalysis data have become available [*Uppala et al.*, 2005], past observational studies focused on the 1979–2001 period, because it is the period during which satellite data have been assimilated in the reanalysis [*Crooks and Gray*, 2005]. A set of simulations was run with the preceding version of WACCM, WACCM3.1 at the same horizontal resolution, and transient forcings, although without the inclusion of a nudged QBO and volcanic eruptions. We compare the solar signal in temperature obtained from WACCM3.5 with that from its preceding version (WACCM3.1) and ERA-40 data sets over the 1979–2001 period [e.g., *Crooks and Gray*, 2005]. The regression model applied to ERA-40 data uses the same QBO regressors as in WACCM3.5 (see (1)), which are based on the first and second EOFs in the QBO domain. To account for the differences in the experimental design, we exclude the QBO and volcanic regressors from the model applied to WACCM3.1. Figure 3 plots solar regression coefficients in temperature from WACCM3.5 (Figure 3a), WACCM3.1 (Figure 3b), and ERA-40 (Figure 3c).

[33] Figure 3c reproduces the same structure shown by *Crooks and Gray* [2005] and *Frame and Gray* [2010], although the regression model applied here is not identical. It is evident from Figures 3a and 3b that both WACCM versions simulate a statistically significant response throughout the stratosphere, characterized by a maximum in the upper stratosphere–lower mesosphere region. At these altitudes, the solar-induced warming peaks at high latitudes, and the warming at low latitudes reaches 0.80 $\pm$ 0.10 K/100 sfu, with slightly higher values in WACCM3.5. These results do not differ from previous equilibrium simulations using WACCM3.1 [*Marsh et al.*, 2007; *Matthes et al.*, 2010] and other CCMs [*Tourpali et al.*, 2003; *Egorova et al.*, 2004; *Austin et al.*, 2008; *Schmidt et al.*, 2010], which suggests that other sources of variability do not affect the results in this region. Figure 3c reveals that a strong warming in the tropical stratopause is also present in ERA-40 data, although the warming in this data set is stronger and limited to low latitudes. In the tropical stratosphere, ERA-40 shows a relative minimum at 30 km, and a significant warming in the lower stratosphere (20 km), with a threefold structure composed by a maximum in the equatorial tropopause, and 2 distinct maxima at a slightly higher altitude in the subtropics with values of 0.80 $\pm$ 0.25 K/100 sfu.

[34] The SC temperature response in WACCM3.5 (Figure 3a) at 20 km is in better agreement with ERA-40 than WACCM3.1 (Figure 3b). In this region, we note that the amplitude of the solar signal in WACCM3.5 is stronger than in the full period (Figure 2a). A similar sensitivity of the response to the analyzed period was noted in WACCM3.1 for tropical ozone [*Marsh and Garcia*, 2007]. They showed that over a relatively short period (e.g., 1979–2003), ENSO may contaminate the solar signal in ozone. However, a separate analysis revealed that excluding the ENSO term in the regression model for WACCM3.5 does not alter our results, which differs from *Marsh and Garcia*'s [2007] results.

[35] Unlike ERA-40 and WACCM3.5, the temperature response in WACCM3.1 in the middle tropical stratosphere is significant. This is probably due to the absence of the QBO in these simulations, which reduces the variability of the temperature field in this region. The WACCM3.1 model shows a weak secondary maximum at 20 km, but there is not evidence of a threefold structure found in ERA-40.

[36] In WACCM3.1, the warming in the lower tropical stratosphere did not appear in previous equilibrium simulations [*Marsh et al.*, 2007; *Tsutsui et al.*, 2009]. With the inclusion of a QBO in the same model version, *Matthes et al.* [2010] reproduced a secondary maximum, whose amplitude is modulated by the QBO phase. However, the magnitude and the structure of the solar signal in temperature at low latitudes in their simulations are not in agreement with that obtained with ERA-40 data shown in Figure 3c.

[37] In the troposphere, both the WACCM ensemble and ERA-40 data show significant warming bands with values of approximately 0.20 $\pm$ 0.05 K/100 sfu at midlatitudes in the NH. The structure of the solar signal in tropospheric in temperature obtained by the regression method in WACCM3.5 is a robust feature since it appears in all ensemble members (not shown).

[38] Figure 4 shows the tropical mean (25°N–25°S) vertical profile of the relative ozone solar regression coefficients in both WACCM ensembles (red and black lines), and the weighted average of three independent satellite instruments presented by *Soukharev and Hood* [2006] (blue line), along with standard error bars for each data set. The satellite data show a relative ozone increase, with a two peak structure with maxima of approximately 2.5% $\pm$ 1.0%/100 sfu at 45 km, a relative minimum at 30 km, and a peak ozone response of more than 3% $\pm$ 2%/100 sfu in the lower tropical stratosphere at 50 and 70 hPa. *Lee and Smith* [2003] showed that the relative minimum response in the middle stratosphere may be due to aliasing of QBO and volcanic signals in ozone. This artifact may affect the results from WACCM3.5 since QBO and volcanoes are included in the simulations but not in WACCM3.1. Both WACCM models show an ozone response, which is broadly similar to that obtained from satellite data, although the structure in the middle and upper stratosphere is slightly shifted toward lower levels with respect to the satellite data.

[39] Interestingly, 2-D and general circulation models show the same discrepancy in the vertical profile of the tropical ozone response [*Rozanov et al.*, 2004; *McCormack et al.*, 2007; *Austin et al.*, 2008], as WACCM runs have revealed. It was speculated that this could be due to the coarse vertical resolution of satellite retrievals for ozone [*Austin et al.*, 2008]. At upper and middle stratospheric levels, the increase in UV radiation during peaks of solar activity favors chemical reactions, which in turn lead to an increase in ozone production [*Pap et al.*, 2003].

[40] The ozone response in WACCM3.5 at 50–70 hPa reaches values up to 3.2%–3.5% $\pm$ 1.0%/100 sfu, which is close to the observed values, while WACCM3.1 simulates a much weaker ozone response, as already shown in Figure 3b for temperature. This improvement of WACCM3.5 over WACCM3.1 is robust at the 50 hPa level, whereas at 70 hPa the uncertainty in the satellite data overlaps the range given by both WACCM models. It should be noted that the satellite data also show high levels of uncertainty. Most of the 2-D models do not show any evidence of a tropical secondary maximum [*Lee and Smith*, 2003; *Smith and Matthes*, 2008],

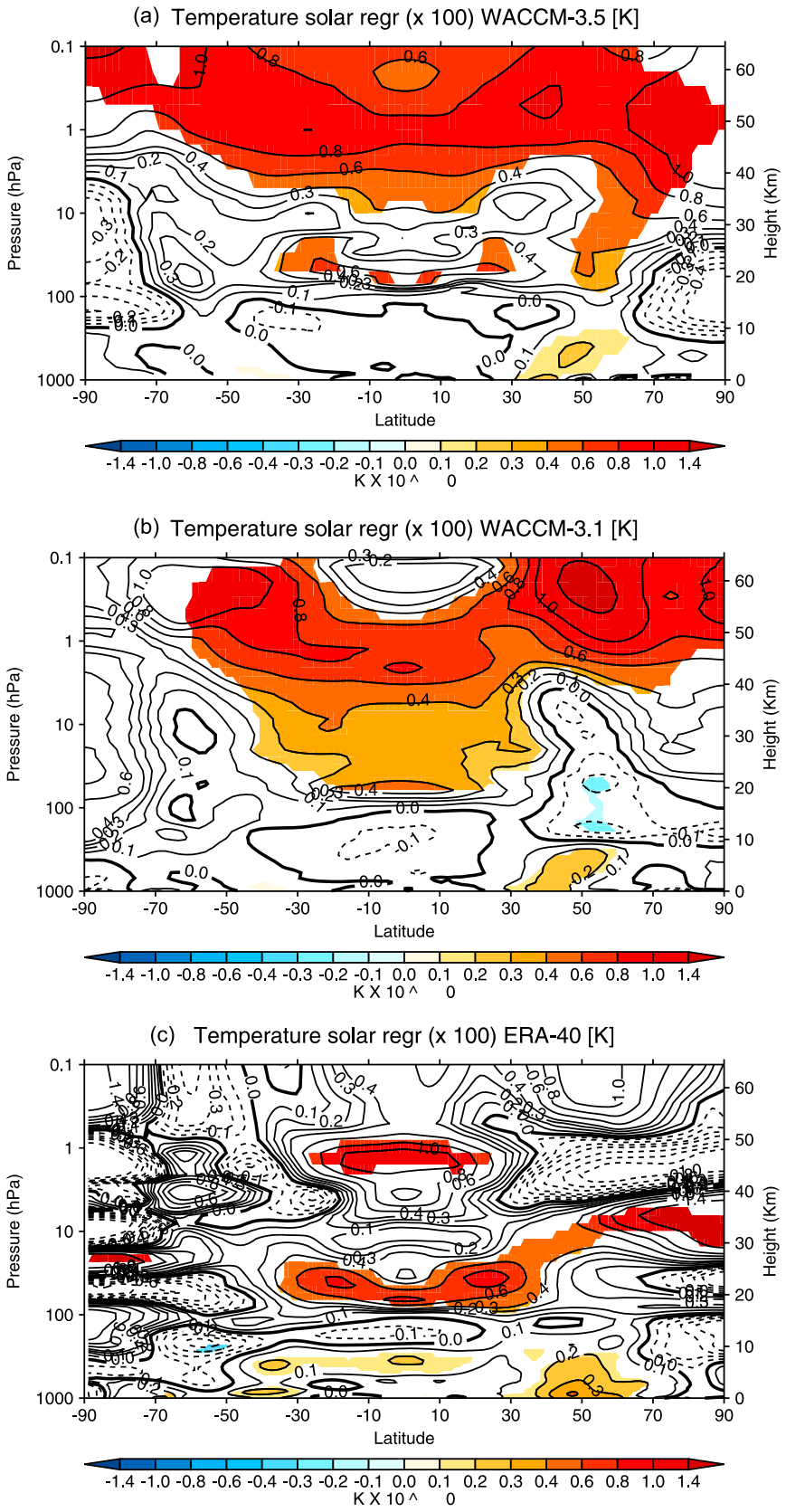

Figure 3. Solar cycle response in zonal mean temperature, displayed as solar regression coefficient ($\times$ 100 sfu) for the period 1979–2001 in (a) WACCM3.5, (b) WACCM3.1, and (c) ERA-40. Colored fields are greater than 2σ. Contours are drawn every 0.1 K. Solid contour lines are drawn to indicate positive values (i.e., warming), while dashed contours indicate negative values (i.e., cooling).

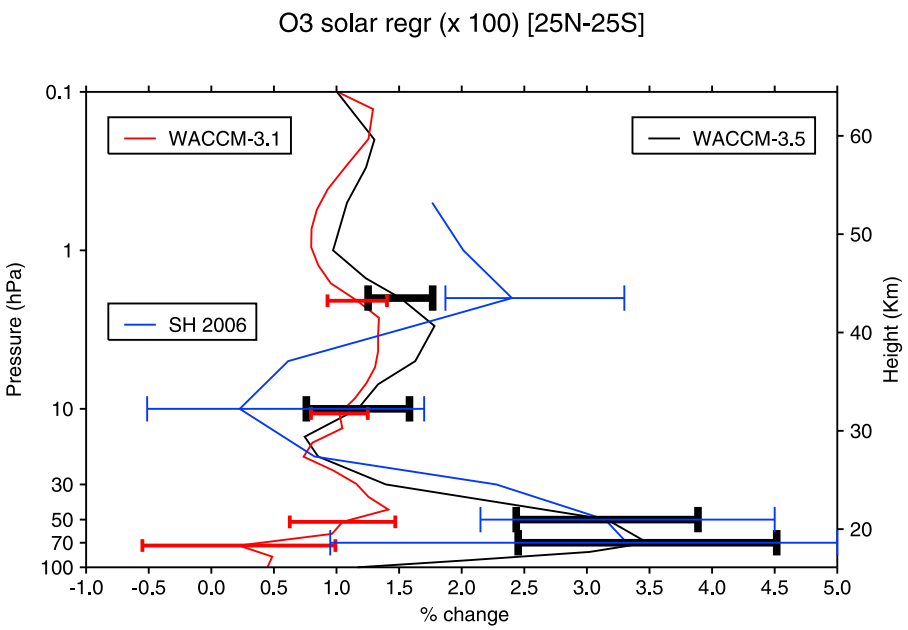

Figure 4. Relative SC response in ozone, displayed as solar regression coefficient of the ensemble mean zonal mean ozone concentration in WACCM3.5 (black), WACCM3.1 (red), and satellite data (blue). The response in satellite data represents the error-weighted mean of three different data sets from *Soukharev and Hood* [2006]. Error bars are drawn to display the 2σ uncertainty in the WACCM simulations and the standard error in satellite data.

while CCMs with comprehensive representation of stratospheric dynamics (e.g., the models used by *Marsh and Garcia* [2007] and *Schmidt et al.* [2010]) simulate a rather weak SC signal in ozone (of the order of 1%–1.5%). At such low stratospheric levels, ozone has a long lifetime, so the increase may be dynamically controlled through changes in vertical upwelling and transport during NH winter, which are investigated in section 4. Hence, the lack of response in some models (especially in 2-D models) could be originated by the missing dynamical feedback in the winter stratosphere.

[41] We tested the possibility of aliasing in the results in the tropical lower stratosphere, as shown by *Marsh and Garcia* [2007]. WACCM3.5 shows some sensitivity of the lower stratospheric ozone response to the reference period, as it occurs in zonal mean temperature. However, the ozone response in WACCM3.5 is stronger than in WACCM3.1 regardless of the length of the data set used in the regression analysis, and of the inclusion of the ENSO term in the regression model.

[42] In addition, the QBO modulation of the solar signal in the ensemble mean zonal mean temperature and ozone in the tropical lower stratosphere (30–50 hPa) is especially noticeable in the easterly phase of the QBO (not shown). The sign and the magnitude of the modulation agrees well with NCEP/NCAR reanalysis [*Labitzke*, 2004]. However, this modulation is not reproduced in all realizations, which indicates that this effect is not a robust feature in the WACCM3.5 simulations.

[43] Figure 5 shows the annual cycle of the solar regression coefficient in the lower stratosphere at 70 hPa as a function of latitude, calculated with ensemble mean zonal mean temperature in WACCM3.5. It is evident that the solar-induced warming of the lower stratosphere seen in Figure 2a has a seasonal cycle, with maximum values in September and December over the equator. Weaker but significant values are also found between 30°N and 45°N from October to January. No evidence of such seasonality in the SC signal in the lower tropical stratospheric temperature is found in the WACCM3.1 simulations (not shown). In the NH, cooling is found at high latitudes from October to January, and from April to June, although it is not statistically significant. A similar pattern is found in the SH between July and December.

[44] These results suggest that in WACCM3.5 the simulated SC signal in the tropical lower stratosphere is linked to

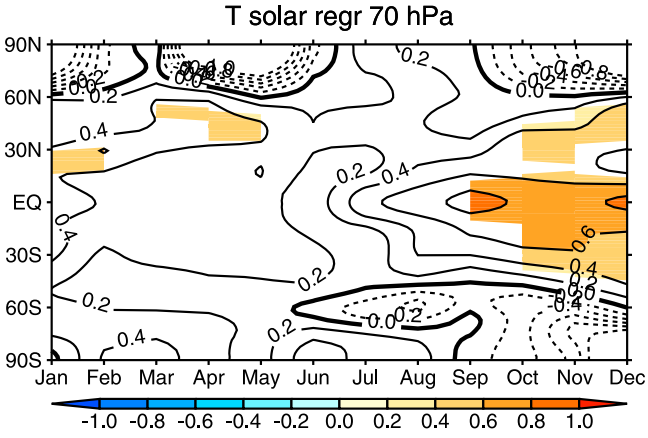

Figure 5. Annual cycle of the zonal mean temperature solar regression coefficient at 70 hPa. Colored fields are greater than 2σ. Contours are drawn every 0.2 K. Solid contour lines are drawn to indicate positive values (i.e., warming), while dashed contours indicate negative values (i.e., cooling).

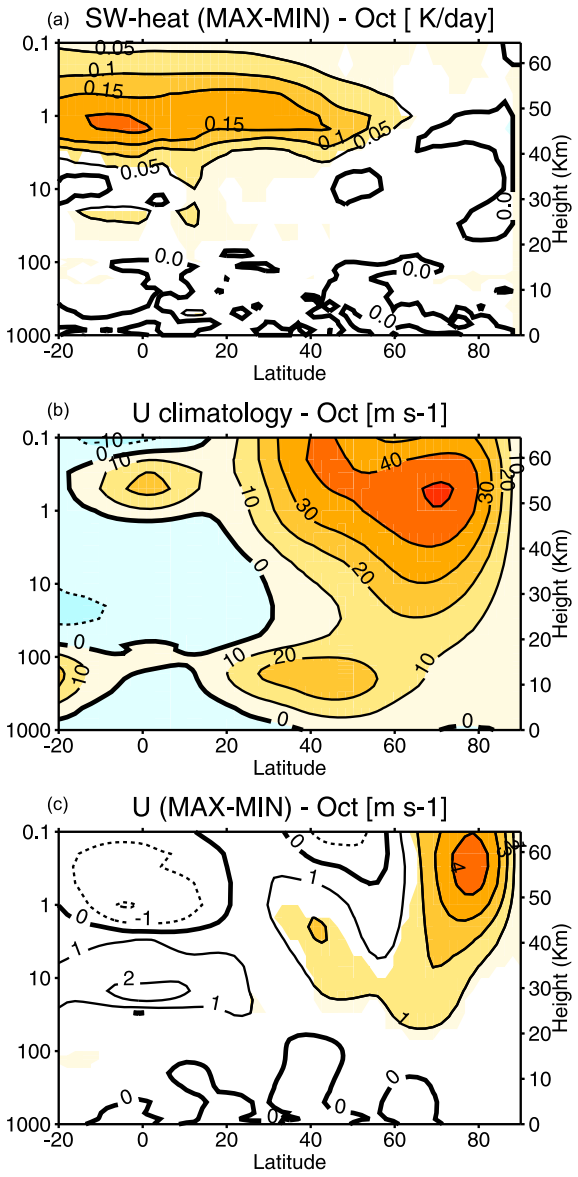

Figure 6. (a) Composite differences (MAX-MIN) of the ensemble mean October monthly mean of zonal mean shortwave heating rate in K/d, (b) zonal wind climatology of the 1960–2005 period in m/s, and (c) as in Figure 6a for zonal mean zonal wind. Shading denotes 95% significant areas; MAX and MIN stand for solar maximum and minimum, respectively.

the SC response at polar latitudes during NH winter and SH spring. For this reason, a detailed analysis of the seasonal evolution of the extratropical solar signal is key in understanding the dynamics of the response at low latitudes shown in this section, and will be shown next.

4. The Solar Signal During Northern Hemisphere Winter

[45] In this section, we present the analysis of the evolution of the SC signal in zonal wind and temperature through the course of the winter season in both hemispheres, with qualitative distinction between direct and indirect responses of the middle atmosphere to the SC.

[46] Figure 6a shows the ensemble mean MAX-MIN composite differences of the model shortwave heating in October. This field is useful to identify the direct model response to the solar forcing. In the upper stratosphere–lower mesosphere (50 km), the solar heating is mainly due to UV absorption by ozone, and it is limited to the tropics and the SH, where the Sun elevation is the highest during the NH fall season (not shown). At low latitudes, the shortwave heating increases by 0.2 K/d during MAX compared to MIN conditions. This is also true during the other fall months (September and November, not shown). This response enhances the meridional temperature gradient at approximately 60°N, where the core of the lower mesospheric jet is located (see Figure 6b). Because of thermal wind balance, the jet significantly increases by around 4 m/s (Figure 6c) during the same month. This is in line with NCEP reanalysis results [*Kuroda and Kodera*, 2001, 2002] and is consistent with the early winter direct solar-induced response mentioned in section 1.

[47] Figures 7 and 8 show MAX-MIN ensemble mean composite differences of the zonal mean zonal wind and temperature from November to February. In November (Figure 7a), the zonal wind anomaly of up to 5 m/s, which was initiated earlier in October by the anomalous UV forcing in the tropical stratopause region, starts to propagate downward to the middle polar stratosphere. The significant zonal wind signal attains its largest magnitude of 6 m/s in the middle polar stratosphere during December (Figure 7b), and negative anomalies appear in the subtropical upper stratosphere, although they are not significant. Weaker (2–4 m/s) but significant positive zonal wind anomalies migrate in January further down into the troposphere with a negative anomalies aloft (Figure 7c), which encompasses the whole polar stratosphere in February (Figure 7d) and March (not shown).

[48] As expected, the response in zonal mean wind is related to that in temperature. In the ensemble zonal mean temperature field (Figure 8), significant warming of up to 4 K develops in November in the polar lower mesosphere (Figure 8a) and propagates downward with height during the following winter months (December, January, and February, shown in Figures 8b, 8c, and 8d, respectively). This is accompanied by cooling at lower levels. Together, they form a vertical dipole structure, which propagates downward. In February (Figure 8d), the warming response is found at 40 km, with weak cooling above and below. The high-latitude temperature response is not significant during most of the winter months because of the high variability caused by the winter SSWs simulated in the model. During November (Figure 8a) and December (Figure 8b), a warming of up to 1 K is also found at low latitudes in the lower stratosphere.

[49] The evolution of the zonal wind signal mostly resembles the observed internal mode of variation of the PNJ [*Kuroda and Kodera*, 2001; *Kodera and Kuroda*, 2002], which indicates that the SC influences the extratropical stratosphere-troposphere system through a modulation of the PNJ oscillation. However, the observed poleward migration of the signal in zonal wind from November to December in the upper stratosphere [see *Kodera and Kuroda*, 2002, Figure 12] is missing in WACCM3.5 and only the downward propagation at polar latitudes is simulated. This is due to the biased position of the lower mesospheric jet in October, which is placed too far toward the pole at 60°N (Figure 6b)

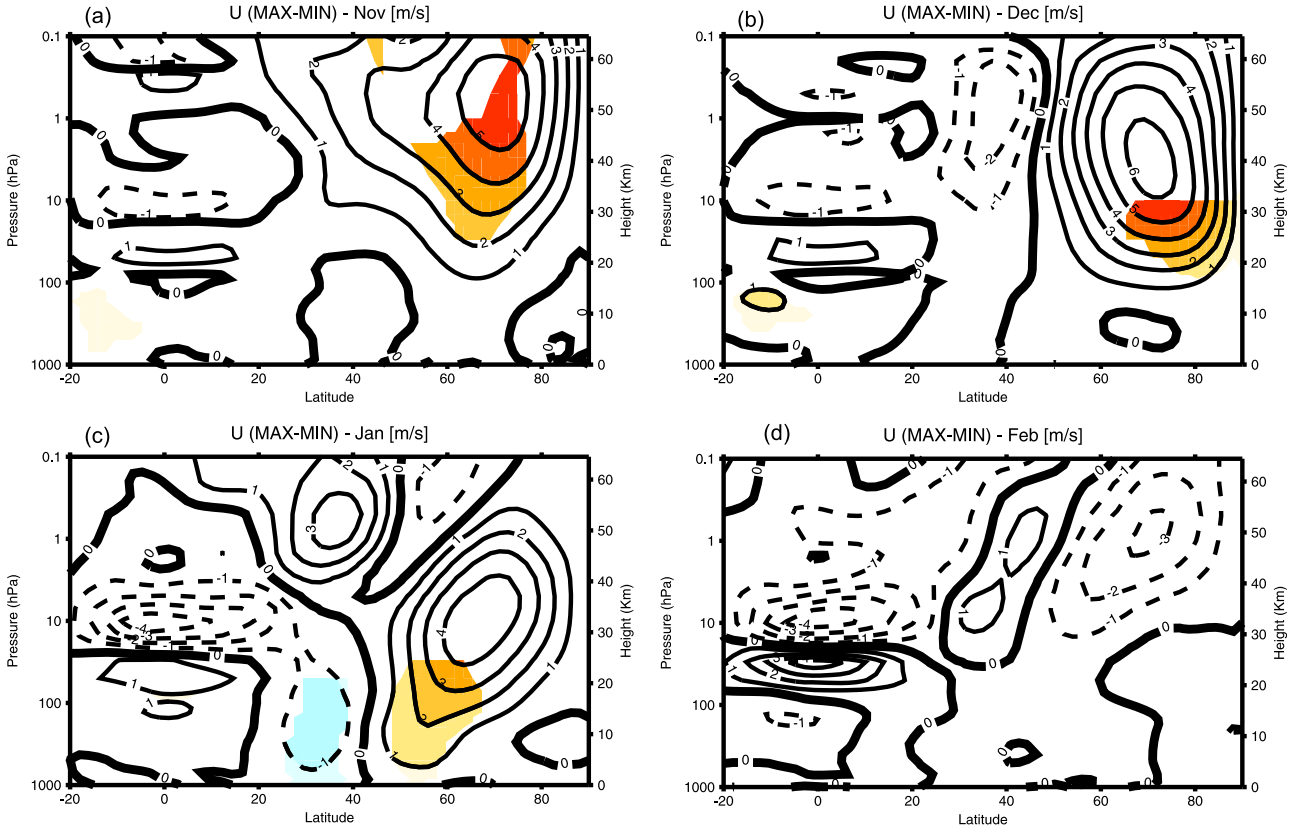

Figure 7. Composite differences (MAX-MIN) of the ensemble mean monthly mean zonal mean zonal wind for (a) November, (b) December, (c) January, and (d) February. Contours are drawn every 1 m/s. Solid contour lines are drawn to display positive (i.e., westerly) values, and dashed contours indicate negative (i.e., easterly) values. Shading denotes 95% significant areas.

compared to observations (not shown). Consequently, the zonal wind anomaly is triggered at midlatitudes instead of in the subtropical upper stratosphere, and propagates downward during the course of the NH winter.

[50] The individual response in zonal wind in the PNJ region (average between 60 and 80°N) can be seen in Figure 9 for each simulation (color lines), which shows the vertical profile of the zonal mean zonal wind MLR solar coefficient for November (Figure 9, top), December (Figure 9, middle), and January (Figure 9, bottom). The same figure also shows the solar regression coefficient of the ensemble mean zonal wind, along with error bars at the 2σ at each vertical model level (black lines). During MAX phases, an increase in zonal mean zonal wind in November (Figure 9, top) is simulated in all ensemble runs, although the magnitude of the wind response and the timing of its subsequent downward propagation varies significantly in each run. This is due to strong variability in some realizations (particularly in run 1 and 4) in December and January, which also explains why the regions of the ensemble mean composite differences are not significant during these months (see Figures 7c and 7d). These are also ensemble members which show a larger number of SSWs (L. De La Torre, personal communication, 2011). The strongest response and the fastest downward propagation of the westerly wind anomaly is found in run 3. Other runs (e.g., run 4) show stronger westerlies during December (Figure 9, middle), but the propagation of the anomalies to the lower levels is slow compared to run 3. Negative (i.e., easterly) anomalies start to appear in January (Figure 9, bottom) in the upper levels (1 hPa) in 2 of the 4 runs, and propagate to the lower levels in February–March (not shown). The strengthening of the PNJ is hence a robust feature of the SC signal in zonal wind in these simulations. Nevertheless, the magnitude of the zonal wind anomalies is uncertain because of large variability of the polar vortex, which is in turn related to the realistic experimental design which includes all observed forcings in the simulations.

[51] These results suggest that maxima of solar activity lead to a stronger polar vortex in November and December. The solar signal in zonal mean zonal wind is initially triggered by stronger UV heating in the upper subtropical stratosphere, and propagates down with the PNJ. In February–March during MAX conditions, the polar vortex weakens. The winter solar signal in zonal wind and temperature in the NH extratropical stratosphere is thus characterized by a transition between different states of the polar vortex. Solar-induced changes in wave-mean flow interactions drive the downward propagation of the stratospheric signal from early to mid winter and the opposite signal in late winter, as explained by *Kodera and Kuroda* [2002] in their conceptual model.

[52] The analysis of the Eliassen-Palm flux (EPF; more details are given by *Andrews et al.* [1987]) and its divergence provides a framework to diagnose and quantify

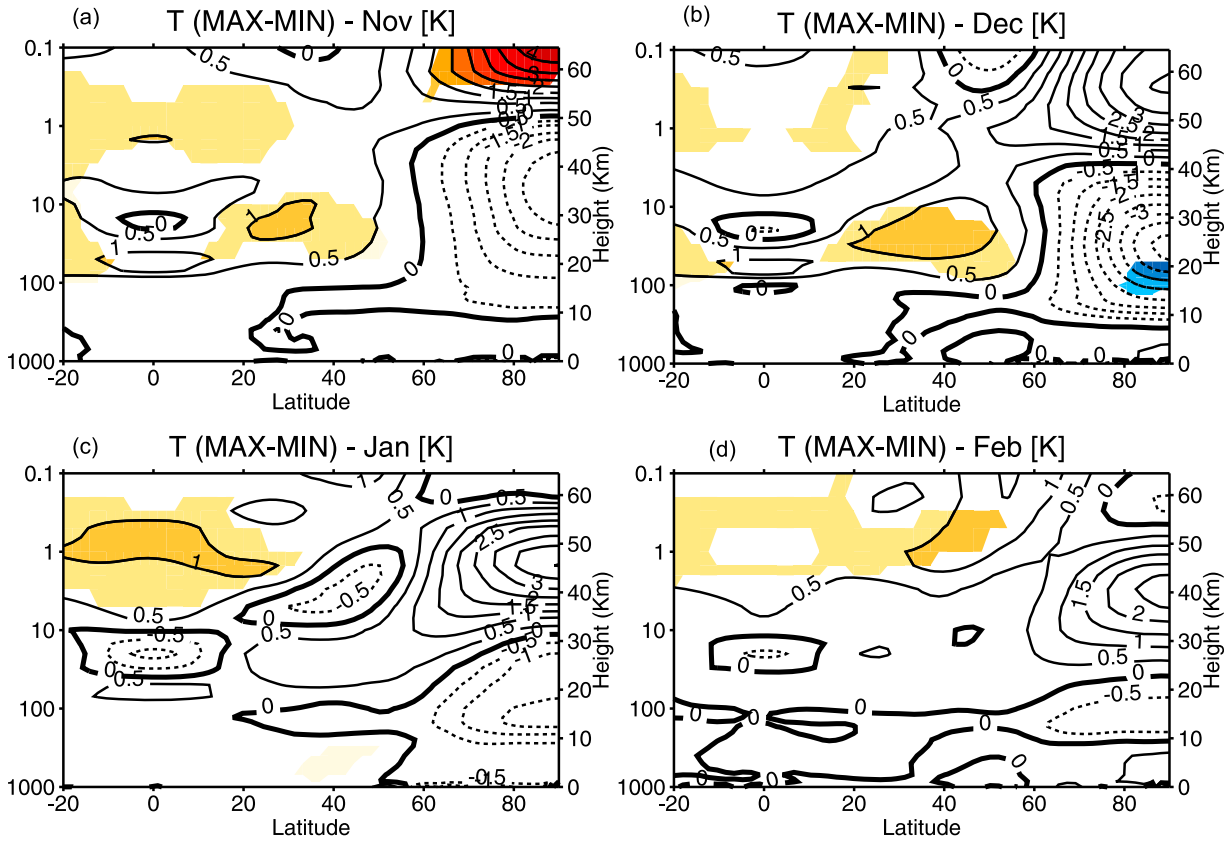

Figure 8. As in Figure 7 for ensemble mean zonal mean temperature. Contour intervals are 0.5 K.

changes in the planetary wave propagation and dissipation, respectively, and therefore to test the mechanisms proposed by *Kodera and Kuroda* [2002]. As a measure for planetary wave activity and wave-mean flow interactions, Figure 10 shows composite differences between MAX and MIN conditions for EPF and its divergence during November (Figure 10a) and December (Figure 10c). Figures 10b and 10d show the composites differences of the transformed Eulerian mean (TEM) meridional ($\bar{v}^*$) and vertical ($\bar{w}^*$) velocities for the same months, which represent the stratospheric mean meridional circulation. During MIN winters, there is upward wave propagation at 60°N from the troposphere into the stratosphere. In the stratosphere, the waves are then refracted toward lower latitudes, and strongly dissipated at higher levels (not shown). During MAX winters, the stronger westerly flow in the middle stratosphere at 60°N observed in November (Figure 7a) reduces the upward propagation of planetary waves in the region, and their equatorward deflection. These anomalies appear as a poleward and downward anomaly (relative to MIN conditions) in the composite differences (Figure 10a). Therefore, less dissipation occurs in this area as indicated by significant positive anomalies in the EPF divergence (2–2.5 m/s/d) simulated at midlatitudes at 50 km (color contours in Figure 10a). This leads in turn to anomalous relative counterclockwise motion in the middle and upper stratosphere, as seen in the TEM velocity vectors in Figure 10b, which act against the characteristic boreal winter stratospheric circulation. This implies that MAX conditions lead to weaker stratospheric residual circulation in November. Less meridional heat transport (not shown) and relative upwelling motion are simulated throughout the whole polar stratosphere (indicated by significant positive anomalies in $\bar{w}^*$ of 0.8 mm/s; color contours in Figure 10b), consistent with the significant cooling which develops in the lower polar stratosphere during November and December (Figures 8a and 8b). At low latitudes, relative downwelling motion during MAX conditions causes the weak warming in the subtropical lower stratosphere in November (Figure 8a).

[53] In December, the positive zonal wind anomalies move downward to the polar lower stratosphere (Figure 7b), and equatorward propagation of waves is enhanced in the lower stratosphere between 40 and 60°N in December (Figure 10c). Further aloft in the polar stratosphere, composite differences indicate an increase in upward and equatorward EPF propagation, and significantly stronger EPF convergence at 40 km during MAX conditions. The enhanced wave dissipation forces a negative westerly anomaly at these levels, which propagates poleward and downward in January–February (see Figures 7c and 7d) and reaches the lower stratosphere in March (not shown). The stronger EP flux convergence also leads to relative clockwise residual motion (which implies stronger Brewer-Dobson circulation) in the middle stratosphere during December (Figure 10d) and following late winter months (not shown). Consequently, relative downwelling in the upper polar stratosphere (indicated by negative anomalies in $\bar{w}^*$, which are drawn as color contours) leads to adiabatic warming

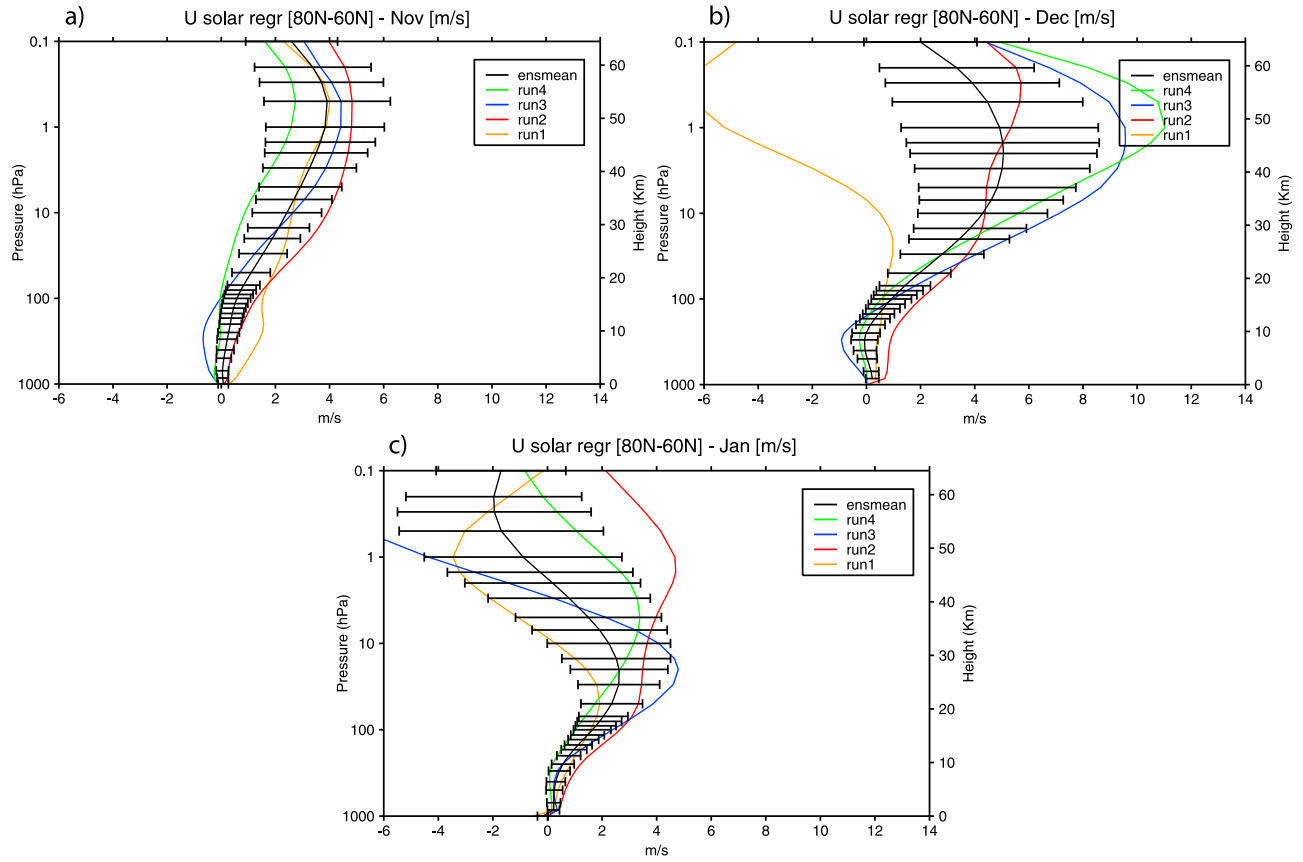

Figure 9. Vertical profile of the polar average (60°N–80°N) zonal wind solar multiple linear regression coefficient for all ensemble runs (colored lines) and ensemble mean (black line) for (a) November, (b) December, and (c) January. Error bars represent the sigma uncertainty range of the regression coefficient for the ensemble mean zonal wind.

in these regions in December. The entire structure propagates downward to the lower stratosphere in late winter (January and February, see Figures 8c and 8d), while stronger upwelling (although weak and not significant) at low latitudes causes slight cooling during MAX conditions between 1 and 10 hPa at midlatitudes and over the Equator during January–February (Figures 7c and 7d). This late winter pattern of warming at high latitudes and equatorial cooling in the stratosphere agrees qualitatively with observations [*Claud et al.*, 2008], although the magnitude of the changes simulated by WACCM3.5 at low latitudes is weaker and not significant.

[54] To summarize, MAX conditions lead to a stronger PNJ in November. The stronger westerlies suppress upward and equatorward planetary wave propagation, and wave dissipation, which in turn leads to a weaker Brewer-Dobson circulation and cooling of the polar stratosphere. In December, when the westerly wind anomaly reaches the lower extratropical stratosphere, upward and equatorward wave propagation is enhanced, along with wave dissipation in the middle stratosphere, leading to a stronger Brewer-Dobson circulation, which stays until March (not shown). Accordingly, the SC signal in the polar stratosphere during winter exhibits a seasonality, which is controlled by changes in wave propagation and dissipation patterns.

[55] Simulations of the SC response with the previous WACCM3.1 model version [*Calvo and Marsh*, 2011] showed a zonal wind anomaly in the equatorial stratopause similar to that in WACCM3.5 (Figure 6c). However, the anomaly did not migrate poleward and downward, thus leading to a weak response in the polar vortex. This was also found by *Tsutsui et al.* [2009]. During October and November, the structure of the PNJ in WACCM3.5 is more realistic than in WACCM3.1, particularly at the polar stratopause (not shown). In WACCM3.1, the PNJ shows a slanted tilt between the subtropical and the high-latitude stratosphere, which is not seen in ERA40 [see *Calvo and Marsh*, 2011, Figure 6]. The more pronounced vertical tilt of the PNJ in WACCM3.5 favors more effective upward propagation of planetary waves in the polar stratopause than in WACCM3.1. The solar-induced changes in zonal wind affect the vertical propagation of planetary waves as shown by *Calvo and Marsh* [2011], which is better represented in WACCM3.5 because of the improved wind climatology in the stratopause region, where the initial change in zonal wind is triggered (Figure 6c).

[56] Furthermore, *Richter et al.* [2009] showed that the stratospheric jet in WACCM3.1 is too strong. Moreover, the overall frequency of major SSWs in this version is low compared to ERA-40 and WACCM3.5. It is thus plausible that an overly strong stratospheric westerly jet might suppress dynamically induced solar changes in WACCM3.1. In the WACCM3.5 simulations presented here, the ensemble mean number of major SSWs agrees with ERA-40 (29.2 in

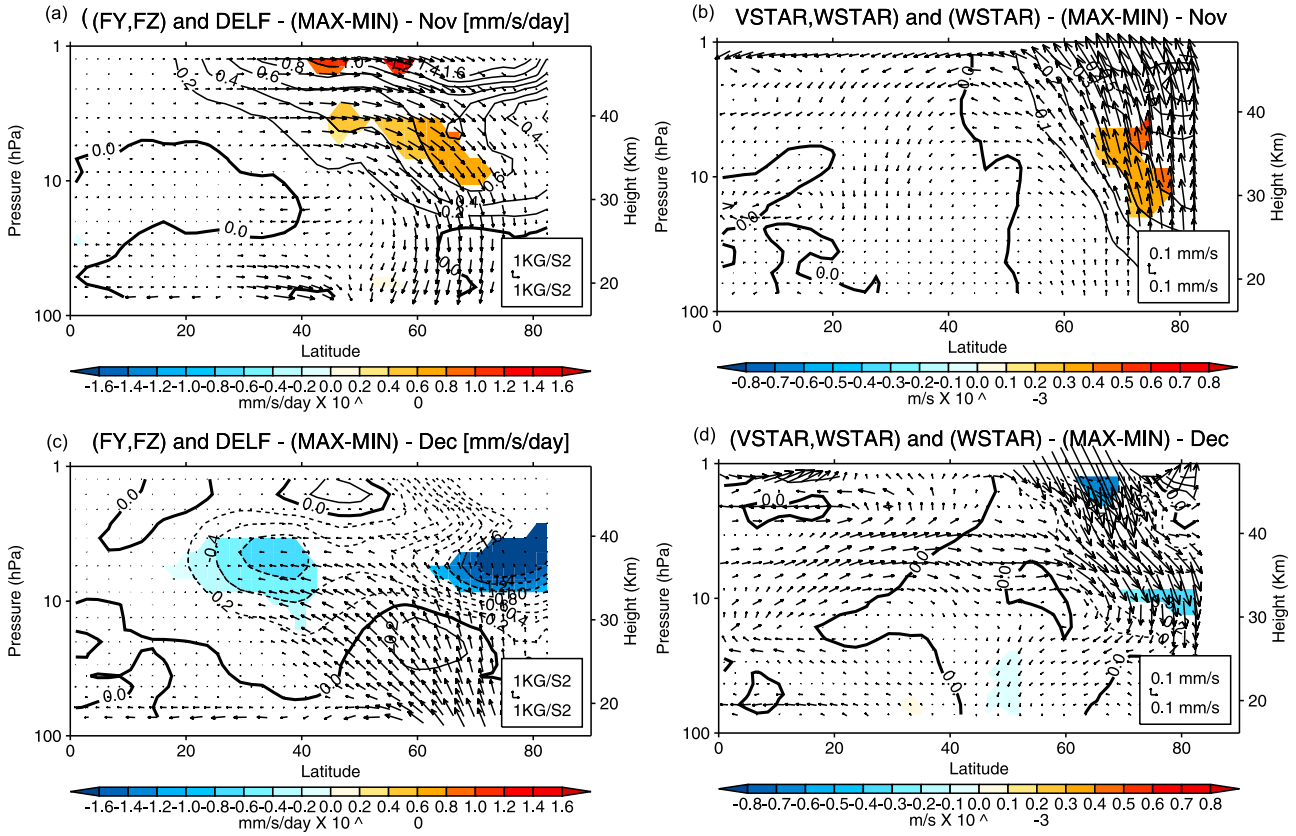

Figure 10. Left panels show the composite differences (MAX-MIN) of the ensemble mean Eliassen-Palm fluxes (EPF) (arrows; Fy and Fz) and EPF divergence for (a) November and (c) December. Units are kg/s for EPF and mm/s/d for EPF divergence. Contours are drawn for the EPF divergence. The composite differences (MAX-MIN) of the ensemble mean transformed Eulerian mean (TEM) velocity vectors (arrows; $\bar{v}^*$ and $\bar{w}^*$) and $\bar{w}^*$ as contours (positive values indicate upwelling, and negative values indicate downwelling) for (b) November and (d) December. Units are mm/s for $\bar{w}^*$. Shading denotes 95% significant areas.

WACCM3.5, and 29 in ERA-40). Notwithstanding the uncertainty in the response of each ensemble member, the more realistic representation of the stratospheric jet and of its variability in the NH polar region is likely to be the basis for the simulation of a realistic solar signal during boreal winter in the newer version of WACCM.

[57] *McCormack et al.* [2007] reproduced a similar SC signal to WACCM3.5 during NH winter. However, since their model cannot incorporate wave-mean flow feedbacks, the changes in the propagation properties of planetary waves due to changes in the mean flow are not accounted for in their model. Previous modeling studies based on CCMs [*Rozanov et al.*, 2004; *Schmidt et al.*, 2010] showed a stronger polar vortex throughout the boreal winter. Other authors simulated the detailed evolution of the boreal winter signal in zonal wind and temperature [*Tourpali et al.*, 2003; *Matthes et al.*, 2004]. However, these simulations were performed with idealized constant forcings. Unlike these past modeling studies, WACCM3.5 reproduces the observed evolution of the winter signal in detail using a set of transient (observed) forcings. This means that the solar-induced response can be reproduced in a model which simulates a more realistic dynamical variability of the winter stratosphere.

[58] In the SH, MAX conditions lead to a meridional dipole of stronger and weaker westerlies at the stratopause during austral winter months (not shown). The dipole propagates downward during austral spring and a weakening of the Brewer-Dobson circulation is found in the SH similar to that found in November and December in the NH. This originates the significant warming in the low tropical stratosphere during September (Figure 5). However, the wind anomalies in the SH are smaller than those simulated in the NH during winter and not statistically significant. Furthermore, they do not penetrate to the lower stratospheric and tropospheric levels, in contrast with observations [*Kuroda and Kodera*, 2002].

[59] This may be a consequence of the biases in the background climatology of the winter stratospheric jet, which were mentioned in section 1. It is plausible that too strong westerlies in the SH modify wave mean flow interactions, and suppress dynamically induced solar changes.

4.1. Influence of the QBO on the Extratropical Solar Signal

[60] In section 3, we investigated the QBO modulation of the SC signal in the tropics in annual mean temperature by using the composite analysis technique, and stratifying the data by both QBO and solar activity phases. A number of studies have analyzed the SC-QBO interactions in the extratropics in observations [*Labitzke*, 1987; *Labitzke and*

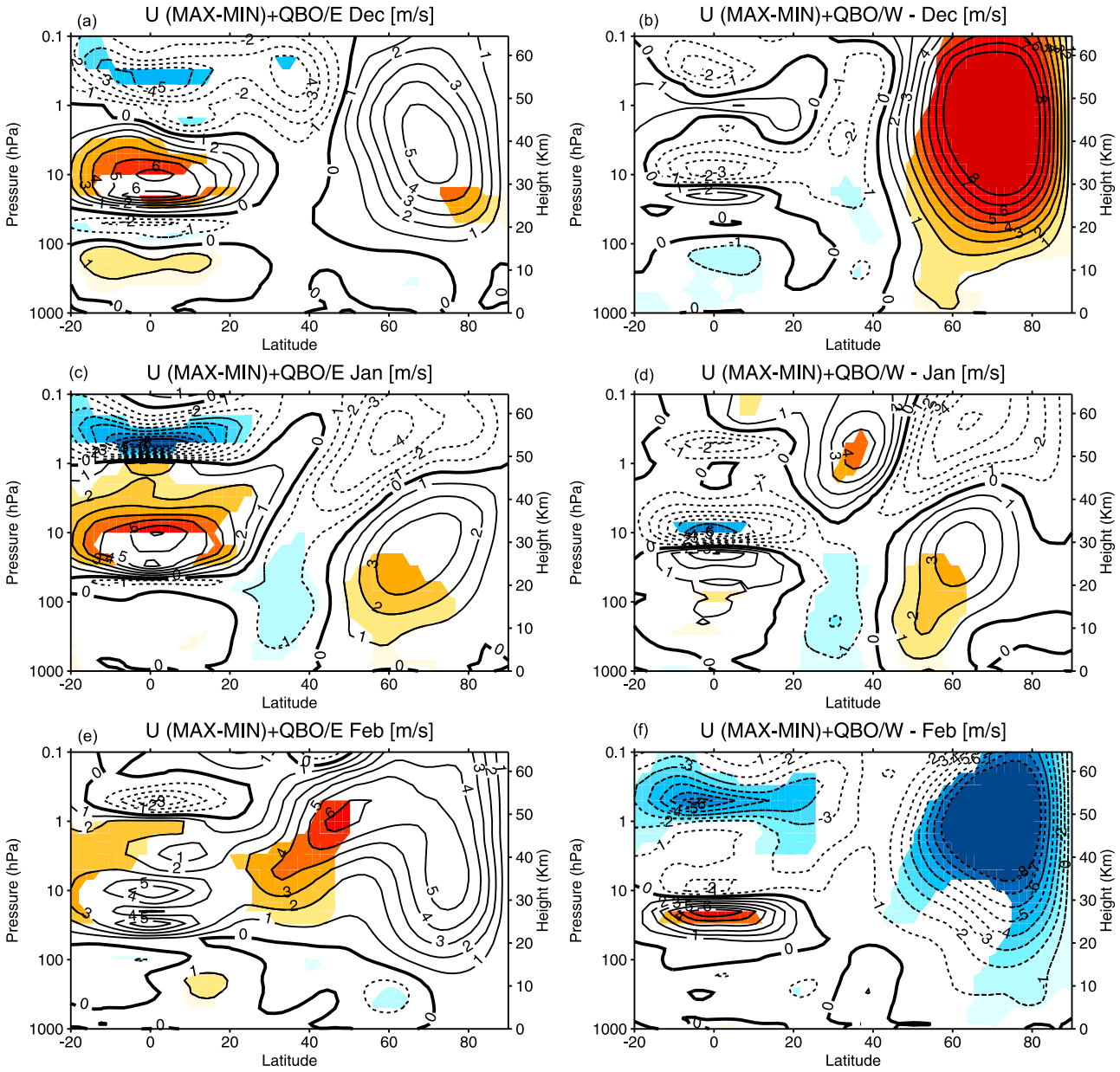

Figure 11. Ensemble mean composite differences (MAX-MIN) of zonal mean zonal wind for (left) QBO/EAST and (right) QBO/WEST winters. Composite differences are shown for (a, b) December, (c, d) January, and (e, f) February. Solid contour lines are drawn to display positive (i.e., westerly) values, and dashed contours indicate negative (i.e., easterly) values. Contour interval is 1 m/s.

Van Loon, 1989] and models of various complexity [*Gray et al.*, 2004; *Schmidt et al.*, 2010; *Matthes et al.*, 2010], and in the context of idealized simulations [*McCormack et al.*, 2007; *Ito et al.*, 2009]. The modeling results concerning combined SC-QBO effects in the polar vortex do not always agree, which may in part be related to the experimental design.

[61] Before analyzing the SC-QBO interactions, we first study the QBO signature in the extratropical stratosphere. To do so, we composited the model anomalies with respect to the ensemble mean climatology according to their QBO phase (QBO/WEST and QBO/EAST), without stratifying data by the solar phase, and selecting winters according to the QBO index in December, as explained in section 2.2. During boreal winters in QBO/WEST phase, the polar vortex is found to be stronger in the ensemble mean, and the opposite occurs during QBO/EAST winters. This indicates that the observed HT relationship [*Holton and Tan*, 1980] is well reproduced in these simulations. However, this pattern was only found in November and December (not shown). During January, February and March the QBO signal in the ensemble mean zonal mean zonal wind switches sign, and therefore a stronger and colder polar vortex is simulated during QBO/EAST (not shown). The modulation of the extratropical QBO signature by the SC can be analyzed when the QBO signal in zonal wind is stratified by the solar phase. We found that the HT relationship is true regardless of the solar phase during early winter. During late winter, the relationship holds true

only in MIN winters, suggesting that the SC does modulate the late winter QBO signal in the polar vortex.

[62] To investigate the modulation of the SC signal in zonal wind by the QBO, ensemble mean composite MAX-MIN differences have been computed for QBO/WEST and QBO/EAST phases throughout the winter, and are shown in Figure 11 from December to February. The SC signal does not depend on the QBO during December (Figures 11a and 11b). This means that MAX conditions lead to stronger ensemble mean zonal wind (i.e., stronger polar vortex) during early winter, regardless of the QBO phase. In January, the westerly wind anomaly propagates to the lower stratospheric levels in both QBO phases (Figures 11c and 11d). In February, MAX conditions lead to significantly stronger ensemble mean zonal wind in QBO/EAST winters (Figure 11f), while easterly anomalies (i.e., weaker polar vortex) are found in QBO/WEST winters (Figure 11e). Therefore, the solar signal in the boreal polar vortex, and its switch from westerly to easterly anomalies (seen in Figures 7b and 7d) is modulated by the QBO phase in late winter. This means that the polar vortex is stronger throughout winters in QBO/EAST phase. No evidence of such QBO modulation of the SC signal during winter is found in the SH (not shown).

[63] In observations, several studies found a similar modulation of the SC by the QBO in the NH [*Labitzke*, 1987; *Labitzke and Van Loon*, 1989]. *McCormack et al.* [2007] obtained similar results to the present study with a 2-D model for QBO/EAST conditions, though their model does not show a clear weakening of the vortex in QBO/WEST conditions (see their Figure 11). The results from the WACCM3.5 simulations were obtained when compositing the ensemble mean zonal wind data, but could not be confirmed in each of the four ensemble simulations. An analysis of the single ensemble runs revealed that only two show differences in the solar signal (MAX-MIN) in zonal wind between both QBO phases during middle and late winter. This indicates that the combined QBO and SC signals in the polar vortex are smaller than internal variability. This occurs even though the statistical *t* test on the ensemble mean fields could indicate a significant modulation of the SC by the QBO, which is close to observations. In addition, the possibility of contamination from the QBO signal cannot be excluded in the SC signal shown in Figures 11e and 11f since a QBO-like structure appears in the tropical stratosphere. Since the tropical winds are assimilated, this could also indicate that a modulation of the QBO itself by the SC [*Salby and Callaghan*, 2000] may intrinsically be introduced in the model simulations. However, further exploration of this modulation is beyond of the scope of this paper.

4.2. Tropospheric Response to the Solar Signal

[64] In the troposphere, Figure 2b showed a dipole of zonal wind anomalies in the ensemble annual mean in the NH as a response to peaks of solar activity. This dipole structure has stronger westerlies at midlatitudes and weaker westerlies in the subtropics, which suggests a weakening and northward shift of the subtropical tropospheric jet. The pattern is prominent in the NH during January (see Figure 7c), although a similar pattern is also simulated in the SH but it is weaker in intensity (not shown). All runs show that this pattern attains its largest magnitude in the upper troposphere–lower stratosphere region in January at 30°N (which is evident as a significant ensemble mean composite difference of −1 m/s in Figure 7c). The structure of the zonal wind response in the troposphere is similar to that found in ERA-40 data in both hemispheres [*Frame and Gray*, 2010]. However, reanalysis data show a larger weakening of the subtropical jets, particularly in the SH during boreal winter [*Frame and Gray*, 2010].

[65] *Haigh and Blackburn* [2006] suggested that the tropospheric wind response may be caused by a weakening in the eddy momentum flux convergence during MAX conditions but a definitive mechanism for the downward propagation of the solar signal to the troposphere has not been provided yet. Although a clear causal relationship cannot be given here, the enhanced meridional planetary wave propagation and dissipation in the tropopause region at midlatitudes during December (Figure 10c) is likely to be related to the tropospheric zonal wind anomalies in January, which lag the mid winter stratospheric SC signal. This suggests a link in the extratropics between the stratospheric and tropospheric solar response, with the stratosphere leading, which agrees well with earlier modeling studies [e.g., *Kodera and Kuroda*, 2000; *Matthes et al.*, 2006].

[66] The SC responses (MAX-MIN) in the ensemble mean surface pressure and temperature during boreal winter are shown in Figures 12a and 12b, respectively. In the NH, the signature is evident as a meridional dipole structure of negative pressure anomalies over the pole, and positive anomalies at midlatitudes. The meridional pressure gradient is particularly strong in the Atlantic and Pacific sectors at approximately 60°N, where Aleutian and Atlantic Low systems normally dominate the synoptic pressure distribution. This pattern is statistically significant, and reminiscent of a positive Arctic Oscillation (AO) response [*Thompson and Wallace*, 1998]. The surface temperature response shows significant warming over Northern Europe, large parts of Siberia, and the Eastern United States. Strong cooling is found over Northern Canada and the West coast of Canada and Alaska. The temperature patterns are broadly consistent with the surface pressure response, and in agreement with other CCMs [*Rozanov et al.*, 2004]. The stronger westerlies in the Atlantic sector advect mild air masses to the Eurasian continent, while the colder temperatures over Northern Canada are linked to the stronger polar vortex. Hence, the solar activity in the WACCM model influences the NH surface climate through projection onto a typical wintertime variability mode of surface pressure. This is consistent with the reported effect of solar variability on the North Atlantic Oscillation and on blocking activity [*Barriopedro et al.*, 2008], which may be a mechanism by which solar-induced changes in the stratosphere influence European weather regimes [*Lockwood et al.*, 2010]. The timing of the solar modulation of NH surface pressure patterns occurs in conjunction with the downward propagation of the SC signal in zonal wind from the stratosphere to the troposphere that we discussed above, and again indicates a link between the solar-induced changes in the stratosphere and troposphere. In the SH, the late winter SC signals in surface pressure and temperature are less persistent and significant, which may be related to the weaker stratospheric response to the SC in this hemisphere (not shown).

[67] The response in zonal mean vertical (pressure) velocity and precipitation during boreal winter are shown in

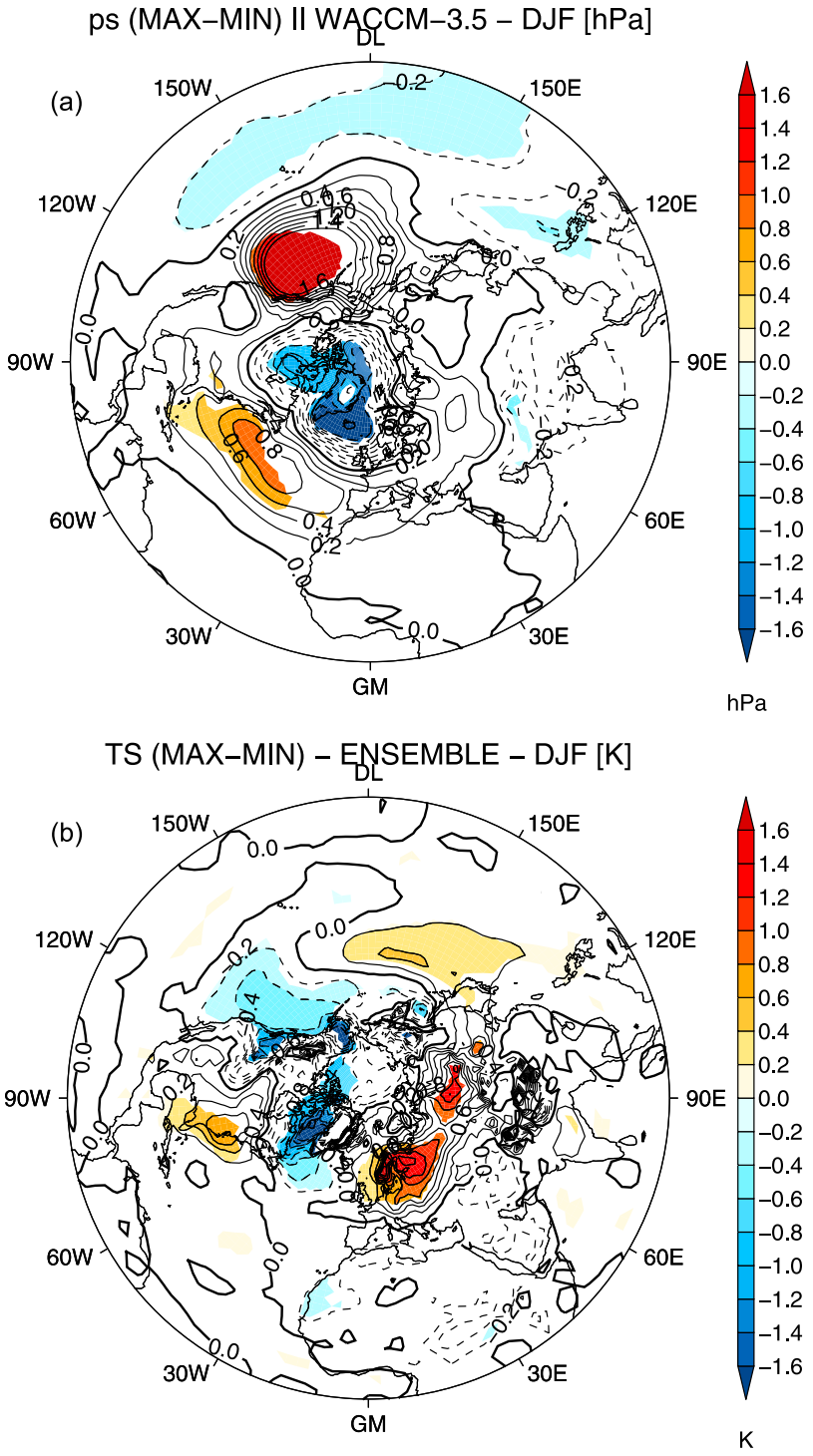

Figure 12. NH winter (DJF) composite differences (MAX-MIN) of (a) ensemble mean surface pressure in Pa and (b) surface temperature in K. Solid contour lines are drawn to indicate positive values (i.e., increase in surface pressure in Figure 12a and surface warming in Figure 12b), while dashed contours indicate negative values (surface pressure decrease in Figure 12a and surface cooling in Figure 12b). Shading denotes 95% significant areas.

Figures 13a and 13b, respectively. Figure 13a shows significant changes in the ensemble mean vertical motion in the tropical middle and lower troposphere. Negative ensemble mean vertical pressure velocity values imply upward changes. The opposite is true for positive changes. We speculate that the simulated warming of the lower stratosphere, which is observed in Figure 2a, leads to an increase of the static stability at the tropopause level. The changes in stability have a strong impact on convection and tropospheric vertical motion, particularly during NH winter. The significant

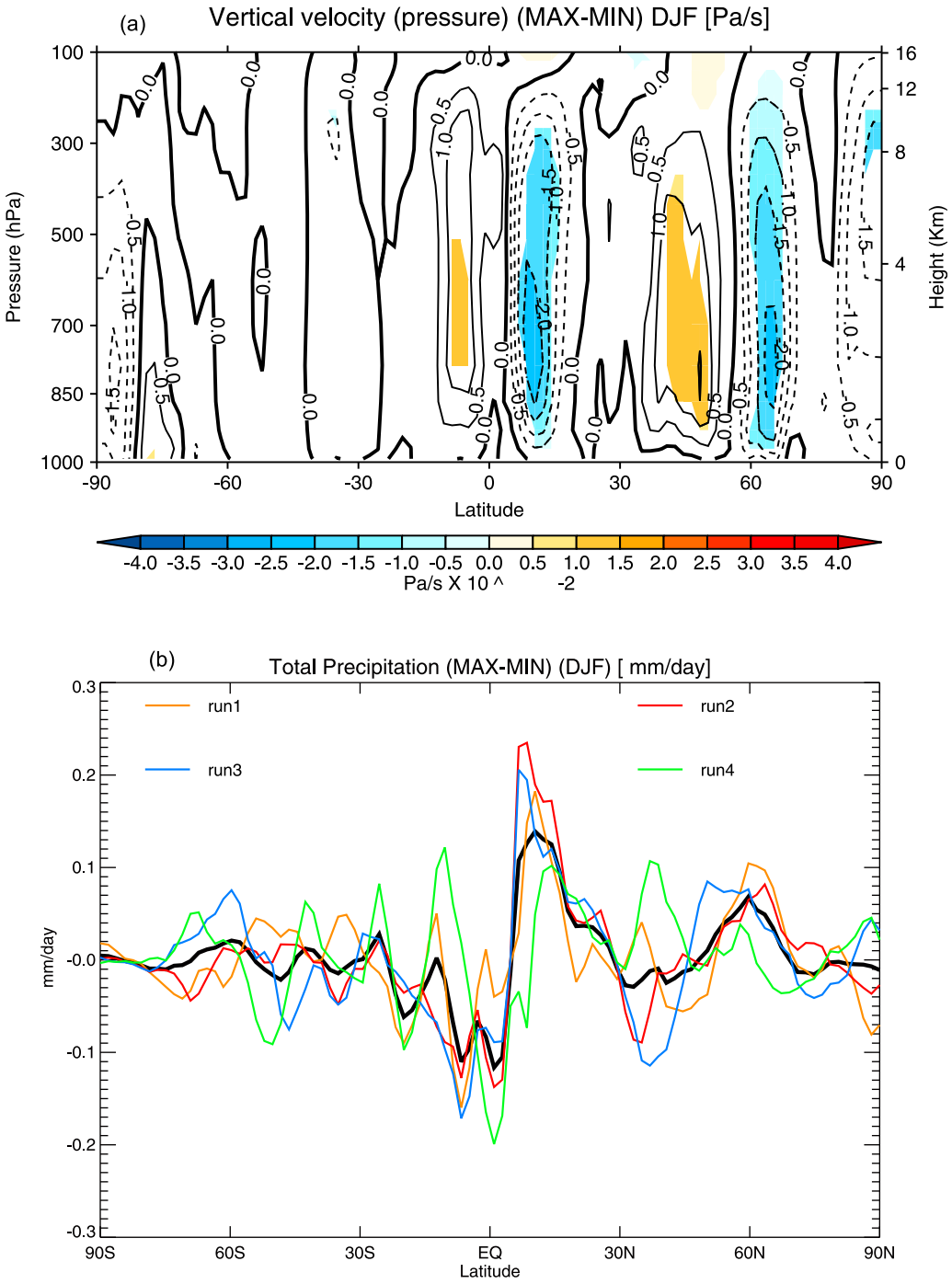

Figure 13. (a) Northern Hemisphere winter (December–February) composite differences (MAX-MIN) of zonal mean pressure velocity (dP/dt) in Pa/s. Solid contour lines are drawn to indicate positive values (i.e., downward anomalies), while dashed contours indicate negative values (i.e., upward anomalies). Shading denotes 95% significant areas. (b) Northern Hemisphere winter (December–February) composite differences (MAX-MIN) of zonal mean total precipitation (convective plus stratiform) for the ensemble mean (black line) and for the single simulations (colored lines) in mm/d.

warming simulated during November in the low equatorial stratosphere supports this hypothesis (Figure 7a). Significant positive changes in the mid troposphere (500–850 hPa) at 10°S indicate a weakening of the climatological upwelling south of the equator during boreal winter, while positive anomalies north of the equator (10–20°N) indicate less downwelling in the downward branch of the Hadley cell. Positive changes at 40–50°N also suggest a northward shift of the downward branch of the Hadley cell in the NH.

[68] These changes occur in conjunction with changes in zonal mean total precipitation, which are shown for the ensemble mean and for each simulation in Figure 13b. The

weaker upwelling leads to less precipitation in the Intertropical Convergence Zone (ITCZ), which lies south of the equator during NH winter at 0°–10°S. The off-equatorial precipitation (10°N) is also intensified during solar maximum conditions. This response in the tropical region is evident in all simulations (although the magnitude of the SC signal in precipitation varies in each one) and suggests that during winters in MAX conditions, the ITCZ is weaker and slightly shifted northward, which agrees well with previous model simulations [*Matthes et al.*, 2006; *Meehl et al.*, 2009]. A similar pattern in tropical precipitation is also found in the NH between July and September, which coincides with a warming in the equatorial lower stratosphere (Figure 5). The weakening and northward shift of the subtropical jet, along with the signals in precipitation and vertical velocity, indicate that in WACCM3.5, MAX conditions lead to a weakening and broadening of the Hadley cell during boreal winter.

[69] Nevertheless, some inconsistency between observational and modeling studies exists concerning the solar-induced response in the tropical circulation [*Gray et al.*, 2010]. Tropospheric solar-induced changes are generally difficult to attribute because of their small size compared to those linked to other sources of variability (e.g., ENSO). The use of observed SSTs implies that ENSO signals may also alias on the decadal response attributed to the SC, as it is the case in tropical SSTs [*White and Liu*, 2008]. A deeper analysis of ENSO aliasing will be discussed in a future study with a more idealized set of forcings.

5. Conclusions

[70] We have analyzed the dynamical SC response in an ensemble of four simulations of the WACCM3.5 chemistry climate model run from 1960 to 2005, which were performed within the coordinated CCMVal-2 activity. Analysis of an ensemble reduces uncertainty in the derived solar signals, which is often larger in transient simulations. In addition, the difference between the ensemble members is a useful metric to assess model uncertainty and robustness of the findings. This improves the detection of the SC signals in various meteorological fields in the stratosphere-troposphere system compared to past GCM studies, particularly in the extratropical region, where indirect solar effects are masked by dynamical variability during the winter season. The main findings are as follows.

[71] 1. The solar signal in annual mean temperature and ozone shows a double-peak response structure in the tropical stratosphere, consisting of warming and ozone increase in the upper and lower levels during solar maximum conditions compared to solar minimum. The signal in the lower stratosphere is closer to observations than in the previous WACCM version.

[72] 2. During solar maximum years, the model simulates a strengthening of the polar vortex in the NH during boreal winter compared to solar minimum conditions. The SC signal in zonal wind and temperature at high latitudes is weak in magnitude, but significant during most of the winter months.

[73] 3. The evolution of the solar signal in zonal wind and temperature in the NH is broadly consistent with observations and conceptual studies. The solar signal in zonal wind shows a downward propagation during early boreal winter in the NH. The response in the polar vortex in late winter is opposite. This is due to opposite changes in planetary wave propagation in early and late winter and related to a different response of the Brewer-Dobson circulation during winters in solar maximum conditions. The winter signal is more realistic than in previous WACCM versions. Part of the improvement is due to the more realistic vertical structure and climatology of the stratospheric jet during winter, and of its variability.

[74] 4. In the polar region, solar maximum conditions lead to a stronger polar vortex in QBO/EAST winters in February, and to a weaker vortex in QBO/WEST winters. The QBO modulation of the tropical and extratropical solar cycle signals in zonal wind agrees well with observations [*Labitzke*, 1987; *Labitzke et al.*, 2006], although it is not reproduced in all ensemble members.

[75] 5. The solar-induced stratospheric anomalies are transmitted to the troposphere in the tropics and extratropics during boreal winter months. In the troposphere, the response to the SC manifests itself as a strong positive AO pattern in the NH midlatitudes, a warming over the Eurasian continent, and as a weakening and broadening of the tropical Hadley circulation.

[76] Overall, WACCM3.5 simulates a realistic solar signal in the tropics and in the NH polar vortex, in better agreement with observations and conceptual studies than WACCM3.1. To our knowledge, no CCM was able, to date, to reproduce the observed solar signal in such agreement in a transient simulation with an evolving solar cycle.

[77] We note that the response to the SC in the upper stratosphere is generally reproduced by a wide range of different models, while more disagreement exists concerning the response in the lower stratosphere, particularly at low latitudes. We have shown indications that solar-induced changes in the polar and low latitude stratosphere are linked through a modulation of the Brewer-Dobson circulation. The better performance of WACCM3.5 compared to WACCM3.1 in both regions is likely to be due to the improvements in the simulation of the boreal winter circulation response. Thus, it is possible that the uncertainty in simulating the solar signal in most models is related to the representation of wave-mean flow interaction processes taking place in the polar stratosphere, which are highly dependent on the background climatology and variability of the polar vortex.

[78] Nevertheless, the simulated changes in the Brewer-Dobson circulation in WACCM3.5 mainly originate high-latitude stratospheric temperature anomalies, whereas the model temperature response at lower latitudes (which would be expected from changes in the upward branch of the residual circulation) is weak and limited to the subtropics. This may be due to the relaxation procedure of observed stratospheric winds in the low equatorial stratosphere (see *Matthes et al.* [2010, section 3.1.1] for details), which forces a secondary QBO circulation that operates independently from the Brewer-Dobson circulation, thus limiting any solar signal in temperature to the extratropics.

[79] This study verifies that the WACCM3.5 model is a suitable model for solar cycle studies, particularly when focusing on the boreal winter circulation response, and on the tropical stratospheric region. The mechanisms responsible for the observed response are well captured by the

model, although a clear causality is still to be determined. The tropospheric signals in different meteorological variables are detectable, although they are small and additional evidence from idealized experiments is still needed.

[80] This study also shows that efforts are still needed to achieve a more realistic simulation of the controversial combined QBO-SC effects in the extratropics. The latter issue could be solved only in future versions of the model where a full interaction between QBO and solar cycle can be investigated by internally generating a QBO in WACCM.

[81] **Acknowledgments.** The authors thank Katja Matthes for instructive comments and fruitful discussions. G. Chiodo was supported by the Spanish Project CONSOLIDER (grant CSD2007-00050-II-PR4/07), TRODIM (grant CGL2007-65891-CO5-02), and the Spanish Ministry of Education in the framework of the "FPU" doctoral fellowship (grant AP2009-0064). N. Calvo was partially supported by the Advanced Study Program (ASP) at NCAR.

References

Andrews, D., J. Holton, and C. Leovy (1987), *Middle Atmosphere Dynamics*, Academic, Orlando, Fla.

Austin, J., et al. (2008), Coupled chemistry climate model simulations of the solar cycle in ozone and temperature, *J. Geophys. Res.*, *113*, D11306, doi:10.1029/2007JD009391.

Austin, J., et al. (2010), Chemistry-climate model simulations of spring Antarctic ozone, *J. Geophys. Res.*, *115*, D00M11, doi:10.1029/2009JD013577.

Barriopedro, D., R. García-Herrera, and R. Huth (2008), Solar modulation of Northern Hemisphere winter blocking, *J. Geophys. Res.*, *113*, D14118, doi:10.1029/2008JD009789.

Butchart, N., A. Charlton-Perez, I. Cionni, S. Hardiman, and K. Krüger (2010), Stratospheric dynamics, in *SPARC Report on the Evaluation of Chemistry-Climate Models*, *SPARC Rep. 5*, pp. 109–147, World Meteorol. Organ., Geneva, Switzerland.

Calvo, N., and D. Marsh (2011), The combined effects of ENSO and the 11-year solar cycle on the Northern Hemisphere polar stratosphere, *J. Geophys. Res.*, *116*, D23112, doi:10.1029/2010JD015226.

Calvo, N., M. Giorgetta, and C. Peña-Ortiz (2007), Sensitivity of the boreal winter circulation in the middle atmosphere to the quasi-biennial oscillation in MAECHAM5 simulations, *J. Geophys. Res.*, *112*, D10124, doi:10.1029/2006JD007844.

Calvo, N., M. Giorgetta, R. Garcia-Herrera, and E. Manzini (2009), Nonlinearity of the combined warm ENSO and QBO effects on the Northern Hemisphere polar vortex in MAECHAM5 simulations, *J. Geophys. Res.*, *114*, D13109, doi:10.1029/2008JD011445.

Claud, C., C. Cagnazzo, and P. Keckhut (2008), The effect of the 11-year solar cycle on the temperature in the lower stratosphere, *J. Atmos. Sol. Terr. Phys.*, *70*(16), 2031–2040.

Collins, W., et al. (2004), Description of the NCAR community atmosphere model (CAM 3.0), *NCAR Tech. Note NCAR/TN-464+ STR*, Natl. Cent. for Atmos. Res., Boulder, Colo.

Crooks, S., and L. Gray (2005), Characterization of the 11-year solar signal using a multiple regression analysis of the ERA-40 dataset, *J. Clim.*, *18*, 996–1015, doi:10.1175/JCLI-3308.1.

Egorova, T., E. Rozanov, E. Manzini, M. Haberreiter, W. Schmutz, V. Zubov, and T. Peter (2004), Chemical and dynamical response to the 11-year variability of the solar irradiance simulated with a chemistry-climate model, *Geophys. Res. Lett.*, *31*, L06119, doi:10.1029/2003GL019294.

Eyring, V., et al. (2010), Multi-model assessment of stratospheric ozone return dates and ozone recovery in CCMVal-2 models, *Atmos. Chem. Phys.*, *10*(19), 11,659–11,710.

Fleming, E., S. Chandra, C. Jackman, D. Considine, and A. Douglass (1995), The middle atmospheric response to short and long term solar UV variations: Analysis of observations and 2D model results, *J. Atmos. Terr. Phys.*, *57*(4), 333–365.

Frame, T., and L. J. Gray (2010), The 11-year solar cycle in ERA-40 data: An update to 2008, *J. Clim.*, *23*, 2213–2222, doi:10.1175/2009JCLI3150.1.

Garcia, R., D. Marsh, D. Kinnison, B. Boville, and F. Sassi (2007), Simulation of secular trends in the middle atmosphere, 1950–2003, *J. Geophys. Res.*, *112*, D09301, doi:10.1029/2006JD007485.

Garcia-Herrera, R., N. Calvo, R. Garcia, and M. Giorgetta (2006), Propagation of ENSO temperature signals into the middle atmosphere: A comparison of two general circulation models and ERA-40 reanalysis data, *J. Geophys. Res.*, *111*, D06101, doi:10.1029/2005JD006061.

Garny, H., G. Bodeker, and M. Dameris (2007), Trends and variability in stratospheric mixing: 1979–2005, *Atmos. Chem. Phys.*, *7*(3), 6189–6228.

Gray, L., S. Crooks, C. Pascoe, S. Sparrow, and M. Palmer (2004), Solar and QBO influences on the timing of stratospheric sudden warmings, *J. Atmos. Sci.*, *61*(23), 2777–2796.

Gray, L., et al. (2010), Solar influences on climate, *Rev. Geophys.*, *48*, RG4001, doi:10.1029/2009RG000282.

Haigh, J. (1994), The role of stratospheric ozone in modulating the solar radiative forcing of climate, *Nature*, *370*(6490), 544–546.

Haigh, J., and M. Blackburn (2006), Solar influences on dynamical coupling between the stratosphere and troposphere, *Space Sci. Rev.*, *125*(1), 331–344, doi:10.1007/s11214-006-9067-0.

Holton, J., and H. Tan (1980), The influence of the equatorial quasi-biennial oscillation on the global circulation at 50 mb, *J. Atmos. Sci.*, *37*, 2200–2208.

Hood, L., J. Jirikowic, and J. McCormack (1993), Quasi-decadal variability of the stratosphere: Influence of long-term solar ultraviolet variations, *J. Atmos. Sci.*, *50*(24), 3941–3958.

Huang, T., and G. Brasseur (1993), Effect of long-term solar variability in a two-dimensional interactive model of the middle atmosphere, *J. Geophys. Res.*, *98*(D11), 413–420, doi:10.1029/93JD02187.

Ito, K., Y. Naito, and S. Yoden (2009), Combined effects of QBO and 11-year solar cycle on the winter hemisphere in a stratosphere-troposphere coupled system, *Geophys. Res. Lett.*, *36*, L11804, doi:10.1029/2008GL037117.

Kalnay, E., et al. (1996), The NCEP/NCAR 40-year reanalysis project, *Bull. Am. Meteorol. Soc.*, *77*(3), 437–471.

Kinnison, D., et al. (2007), Sensitivity of chemical tracers to meteorological parameters in the MOZART-3 chemical transport model, *J. Geophys. Res.*, *112*, D20302, doi:10.1029/2006JD007879.

Kistler, R., et al. (2001), The NCEP-NCAR 50-year reanalysis: Monthly means CD-ROM and documentation, *Bull. Am. Meteorol. Soc.*, *82*(2), 247–268.

Kodera, K., and Y. Kuroda (2000), A mechanistic model study of slowly propagating coupled stratosphere-troposphere variability, *J. Geophys. Res.*, *105*(D10), 361–370.

Kodera, K., and Y. Kuroda (2002), Dynamical response to the solar cycle, *J. Geophys. Res.*, *107*(D24), 4749, doi:10.1029/2002JD002224.

Kuroda, Y., and K. Kodera (2001), Variability of the polar night jet in the Northern and Southern Hemispheres, *J. Geophys. Res.*, *106*(D18), 20,703–20,713.

Kuroda, Y., and K. Kodera (2002), Effect of solar activity on the polar-night jet oscillation in the Northern and Southern Hemisphere winter, *J. Meteorol. Soc. Jpn.*, *80*(4B), 973–984.

Labitzke, K. (1987), Sunspots, the QBO, and the stratospheric temperature in the north polar region, *Geophys. Res. Lett.*, *14*(5), 535–537, doi:10.1029/GL014i005p00535.

Labitzke, K. (2004), On the signal of the 11-year sunspot cycle in the stratosphere and its modulation by the quasi-biennial oscillation, *J. Atmos. Sol. Terr. Phys.*, *66*(13–14), 1151–1157, doi:10.1016/j.jastp.2004.05.011.

Labitzke, K. (2005), On the solar cycle-QBO relationship: A summary, *J. Atmos. Sol. Terr. Phys.*, *67*(1–2), 45–54, doi:10.1016/j.jastp.2004.07.016.

Labitzke, K., and H. Van Loon (1989), Association between the 11-Yr Solar Cycle, the QBO, and the Atmosphere. Part III: Aspects of the association, *J. Clim.*, *2*(6), 554–565, doi:10.1175/1520-0442(1989)002<0554:ABTYSC>2.0.CO;2.

Labitzke, K., and H. Van Loon (1995), Connection between the troposphere and stratosphere on a decadal scale, *Tellus, Ser. A*, *47*(2), 275–286, doi:10.1034/j.1600-0870.1995.t01-1-00008.x.

Labitzke, K., J. Austin, N. Butchart, J. Knight, M. Takahashi, M. Nakamoto, T. Nagashima, J. Haigh, and V. Williams (2002), The global signal of the 11-year solar cycle in the stratosphere: Observations and models, *J. Atmos. Sol. Terr. Phys.*, *64*(2), 203–210, doi:10.1016/S1364-6826(01)00084-0.

Labitzke, K., M. Kunze, and S. Broennimann (2006), Sunspots, the QBO and the stratosphere in the North Polar region—20 years later, *Meteorol. Z.* [Berlin], *15*(3), 355–364, doi:10.1127/0941-2948/2006/0136.

Lean, J., G. Rottman, H. Kyle, T. Woods, J. Hickey, and L. Puga (1997), Detection and parameterization of variations in solar mid-and near-ultraviolet radiation (200–400 nm), *J. Geophys. Res.*, *102*(D25), 29,939–29,956, doi:10.1029/97JD02092.

Lean, J., G. Rottman, J. Harder, and G. Kopp (2005), SORCE contributions to new understanding of global change and solar variability, *Sol. Phys.*, *230*, 27–53, doi:10.1007/s11207-005-1527-2.

Lee, H., and A. Smith (2003), Simulation of the combined effects of solar cycle, quasi-biennial oscillation, and volcanic forcing on stratospheric ozone changes in recent decades, *J. Geophys. Res.*, *108*(D2), 4049, doi:10.1029/2001JD001503.

Lin, S. (2004), A vertically Lagrangian finite-volume dynamical core for global models, *Mon. Weather Rev.*, *132*, 2293–2307, doi:10.1175/1520-0493(2004)132<2293:AVLFDC>2.0.CO;2.

Lockwood, M., R. Harrison, T. Woollings, and S. Solanki (2010), Are cold winters in Europe associated with low solar activity?, *Environ. Res. Lett.*, *5*(2), 024001, doi:10.1088/1748-9326/5/2/024001.

Manzini, E., et al. (2010), Natural variability, in *SPARC Report on the Evaluation of Chemistry-Climate Models*, *SPARC Rep. 5*, pp. 306–346, World Meteorol. Organ., Geneva, Switzerland.

Marsh, D., and R. Garcia (2007), Attribution of decadal variability in lower-stratospheric tropical ozone, *Geophys. Res. Lett.*, *34*, L21807, doi:10.1029/2007GL030935.

Marsh, D., R. Garcia, D. Kinnison, B. Boville, F. Sassi, S. Solomon, and K. Matthes (2007), Modeling the whole atmosphere response to solar cycle changes in radiative and geomagnetic forcing, *J. Geophys. Res.*, *112*, D23306, doi:10.1029/2006JD008306.

Matthes, K., U. Langematz, L. Gray, K. Kodera, and K. Labitzke (2004), Improved 11-year solar signal in the Freie Universitaet Berlin climate middle atmosphere model (FUB-CMAM), *J. Geophys. Res.*, *109*, D06101, doi:10.1029/2003JD004012.

Matthes, K., Y. Kuroda, K. Kodera, and U. Langematz (2006), Transfer of the solar signal from the stratosphere to the troposphere: Northern winter, *J. Geophys. Res.*, *111*, D06108, doi:10.1029/2005JD006283.

Matthes, K., D. Marsh, R. Garcia, D. Kinnison, F. Sassi, and S. Walters (2010), Role of the QBO in modulating the influence of the 11 year solar cycle on the atmosphere using constant forcings, *J. Geophys. Res.*, *115*, D18110, doi:10.1029/2009JD013020.

McCormack, J., and L. Hood (1996), Apparent solar cycle variations of upper stratospheric ozone and temperature: Latitude and seasonal dependences, *J. Geophys. Res.*, *101*(D15), 20,933–20,944, doi:10.1029/96JD01817.

McCormack, J., D. Siskind, and L. Hood (2007), Solar-QBO interaction and its impact on stratospheric ozone in a zonally averaged photochemical transport model of the middle atmosphere, *J. Geophys. Res.*, *112*, D16109, doi:10.1029/2006JD008369.

Meehl, G., J. Arblaster, K. Matthes, F. Sassi, and H. van Loon (2009), Amplifying the Pacific climate system response to a small 11-year solar cycle forcing, *Science*, *325*(5944), 1114–1118, doi:10.1126/science.1172872.

Pap, J., P. Fox, C. Fröhlich, H. S. Hudson, J. Kuhn, J. McCormack, G. North, W. Sprigg, and S. T. Wu (Eds.) (2003), *Solar Variability and Its Effects on Climate*, *Geophys. Monogr. Ser.*, vol. 141, AGU, Washington, D. C., doi:10.1029/GM141.

Randel, W., and F. Wu (1996), Isolation of the ozone QBO in SAGE 2 data by singular-value decomposition, *J. Atmos. Sci.*, *53*(17), 2546–2560, doi:10.1175/1520-0469(1996)053<2546:IOTOQI>2.0.CO;2.

Randel, W., and F. Wu (2007), A stratospheric ozone profile data set for 1979–2005: Variability, trends, and comparisons with column ozone data, *J. Geophys. Res.*, *112*, D06313, doi:10.1029/2006JD007339.

Richter, J., F. Sassi, and R. Garcia (2009), Towards a physically based gravity wave source parameterization in a general circulation model, *J. Atmos. Sci.*, *67*, 136–156, doi:10.1175/2009JAS3112.1.

Rozanov, E., M. Schlesinger, T. Egorova, B. Li, N. Andronova, and V. Zubov (2004), Atmospheric response to the observed increase of solar UV radiation from solar minimum to solar maximum simulated by the University of Illinois at Urbana-Champaign climate-chemistry model, *J. Geophys. Res.*, *109*, D01110, doi:10.1029/2003JD003796.

Salby, M., and P. Callaghan (2000), Connection between the solar cycle and the QBO: The missing link, *J. Clim.*, *13*(14), 2652–2662, doi:10.1175/1520-0442(1999)012<2652:CBTSCA>2.0.CO;2.

Sassi, F., D. Kinnison, B. Boville, R. Garcia, and R. Roble (2004), Effect of El Niño–Southern Oscillation on the dynamical, thermal, and chemical structure of the middle atmosphere, *J. Geophys. Res.*, *109*, D17108, doi:10.1029/2003JD004434.

Sato, M., J. Hansen, M. McCormick, and J. Pollack (1993), Stratospheric aerosol optical depths, 1850–1990, *J. Geophys. Res.*, *98*(D12), 22,987–22,994, doi:10.1029/93JD02553.

Schmidt, H., G. Brasseur, and M. Giorgetta (2010), Solar cycle signal in a general circulation and chemistry model with internally generated quasi-biennial oscillation, *J. Geophys. Res.*, *115*, D00I14, doi:10.1029/2009JD012542.

Shindell, D., D. Rind, N. Balachandran, J. Lean, and P. Lonergan (1999), Solar cycle variability, ozone, and climate, *Science*, *284*(5412), 305–308, doi:10.1126/science.284.5412.305.

Smith, A., and K. Matthes (2008), Decadal-scale periodicities in the stratosphere associated with the solar cycle and the QBO, *J. Geophys. Res.*, *113*, D05311, doi:10.1029/2007JD009051.

Solomon, S., and L. Qian (2005), Solar extreme-ultraviolet irradiance for general circulation models, *J. Geophys. Res.*, *110*, A10306, doi:10.1029/2005JA011160.

Soukharev, B., and L. Hood (2006), Solar cycle variation of stratospheric ozone: Multiple regression analysis of long-term satellite data sets and comparisons with models, *J. Geophys. Res.*, *111*, D20314, doi:10.1029/2006JD007107.

Thompson, D., and J. Wallace (1998), The Arctic Oscillation signature in the wintertime geopotential height and temperature fields, *Geophys. Res. Lett.*, *25*(9), 1297–1300, doi:10.1029/98GL00950.

Tiao, G., G. Reinsel, D. Xu, J. Pedrick, X. Zhu, A. Miller, J. DeLuisi, C. Mateer, and D. Wuebbles (1990), Effects of autocorrelation and temporal sampling schemes on estimates of trend and spatial correlation, *J. Geophys. Res.*, *95*(D12), 20,507–20,517, doi:10.1029/JD095iD12p20507.

Tilmes, S., R. Garcia, D. Kinnison, A. Gettelman, and P. Rasch (2009), Impact of geoengineered aerosols on the troposphere and stratosphere, *J. Geophys. Res.*, *114*, D12305, doi:10.1029/2008JD011420.

Tourpali, K., C. Schuurmans, R. Van Dorland, B. Steil, and C. Brühl (2003), Stratospheric and tropospheric response to enhanced solar UV radiation: A model study, *Geophys. Res. Lett.*, *30*(5), 1231, doi:10.1029/2002GL016650.

Tsutsui, J., K. Nishizawa, and F. Sassi (2009), Response of the middle atmosphere to the 11-year solar cycle simulated with the Whole Atmosphere Community Climate Model, *J. Geophys. Res.*, *114*, D02111, doi:10.1029/2008JD010316.

Uppala, S., et al. (2005), The ERA-40 re-analysis, *Q. J. R. Meteorol. Soc.*, *131*(612), 2961–3012, doi:10.1256/qj.04.176.

White, W., and Z. Liu (2008), Non-linear alignment of El Nino to the 11-yr solar cycle, *Geophys. Res. Lett.*, *35*, L19607, doi:10.1029/2008GL034831.

N. Calvo and D. R. Marsh, Atmospheric Chemistry Division, National Center for Atmospheric Research, PO Box 3000, Boulder, CO 80307, USA.

G. Chiodo, Departamento Fisica de la Tierra II, Facultad de Ciencias Fisicas, Universidad Complutense de Madrid, E-28040 Madrid, Spain. (gchiodo@fis.ucm.es)

R. Garcia-Herrera, Agencia Estatal de Meteorologia, E-28040 Madrid, Spain.